# Structural Characterization of Cross-linked Pluronic Hydrogels via Small Angle X-ray Scattering

Elizabeth Harmon

A thesis

submitted in partial fulfillment of the

requirements for the degree of

Master of Science in Chemical Engineering

University of Washington

2022

Committee:

Lilo Pozzo, Chair

David Beck

Program Authorized to Offer Degree:

Chemical Engineering

University of Washington

**Abstract**

Structural Characterization of Cross-linked Pluronic Hydrogels via Small Angle X-ray Scattering

Elizabeth Harmon

Chair of the Supervisory Committee:
Professor Lilo Pozzo

Department of Chemical Engineering

Engineered living materials (ELMs) are a new technology within Synthetic Biology (SynBio) that incorporates living microbial organisms within hydrogel matrices. Unlike traditional liquid cultures of living cells, both components in engineered living hydrogels can be programmed to meet specific goals. The living cells can be engineered to fulfill a multitude of functions, ranging from sensing to chemical production, and even generation of electricity. Hydrogels are a popular construct for these materials for a number of reasons. Most hydrogels offer a high degree of biocompatibility and chemical permeability that make it ideal for sustaining living microbes. There are a number of design criteria that must be met to determine if the hydrogel platform is a good candidate for manufacturing chemical intermediates. They must be able to provide compartmentalization of living cells, prevent cell leakage, maintain mechanical integrity, allow substrates and products to flow in and out of the hydrogel matrix, and sustain a long shelf life. The primary motivation behind the research presented in this thesis is to contribute to the collaborative effort amongst an interdisciplinary team of researchers funded by the National Science Foundation (NSF). This group is interested in expanding the potential of SynBio and

ELMs by developing next generation bioreactors capable of converting cheap raw materials (such as sugars and amino acids) into high-value products such as pharmaceuticals and chemical intermediates using yeast and bacteria as the biocatalysts. Current manufacturing processes for these chemicals of interest require sourcing materials that rely on unsustainable farming practices. The development of these microbe-laden hydrogels could introduce a more sustainable approach to manufacturing these products. Pluronic F127 was selected as the polymer for this hydrogel due to its relatively high solubility in water and its ability to self-assemble in aqueous media without additives. Pluronic F127 as it exists off the shelf does not fulfill the required design criteria. Although it is capable of gelling, it cannot maintain this mechanical integrity when exposed to solution. Therefore, a new functionalized form of F127, known was F127-BUM, was developed by the Nelson Research Group. The work presented in this thesis focuses on using small angle X-ray scattering to characterize the progression of F127 through functionalization with bisurethane methacrylate to form F127-BUM, polymerization into cured hydrogels to prevent dissolution in water, and lyophilization/rehydration for extended shelf life.

# TABLE OF CONTENTS

# LIST OF TABLES

# LIST OF FIGURES

# Chapter 1: Introduction

## 1.1 Introduction to Hydrogels

Hydrogels are hydrophilic, three-dimensional polymeric networks capable of retaining large amounts of water or biological fluids while also maintaining their structure. The high thermodynamic affinity that this class of materials exhibits toward its solvent (water) leads to a high degree of swelling that has become characteristic of hydrogels[1]. Hydrogels can be classified in several ways. One important classification is based on the origin of the polymer from which it was derived. Natural hydrogels are derived from natural sources, such as alginate, collagen, gelatin, and fibrin[2]. The advantage to manufacturing hydrogels from natural sources is their biocompatibility, biodegradability, and non-toxicity. Synthetic hydrogels, derived from synthetic polymers such as polyacrylamide, polyamides, and polyethylene glycol, have recently been favored over their natural counterparts due to their long life, strength, and greater ability to absorb water[2]. The well-defined structures associated with synthetic hydrogels allow engineers to design systems with better yield, flexible degradability, and functionality[2].

In addition to classifying hydrogels as physical or chemical, they are also classified based on the nature of their cross-linking. Hydrogels are considered physical or reversible gels if the main force holding them together are molecular entanglements or secondary forces, such as electrostatic forces, hydrogen bonds, hydrophobic interactions, or chain entanglements[3]. Physical gels are capable of transitioning between sol and gel states in response to changes in the environmental conditions, such as pH, temperature, ionic concentration, or even the mixture of two components. This means these gels may not maintain structural integrity when exposed to solution[3]. When the network of covalent bonds that joins the polymeric chains has been cross-

linked, these hydrogels are considered permanent, or chemical gels. Cross-linking introduces mechanical integrity and resistance to degradation[3].

## 1.2 Applications of Hydrogels

### 1.2.1 Drug Delivery Systems

Hydrogels are a highly studied platform for many applications ranging from industrial to biological. Hydrogels have shown promising results in controlled drug delivery systems due to the high porosity that can be achieved. These systems are used to deliver drugs to targeted areas in the body and at controlled rates[3]. The porous structures of hydrogels make them highly permeable to different kinds of drugs. These drugs can be loaded in the hydrogel network. Once they are introduced to the harsh conditions of the body, they are protected by the hydrogels until they reach the targeted area. When exposed to certain conditions, which can be controlled by changes in pH, temperature, or the presence of enzymes, they can then be released at a controlled rate (Figure 1). Masayuki Yokoyama et al. have demonstrated that the hydrophilicity of the PEG chains and size (>100 nm) could be used to successfully target a solid tumor with a polymeric micelle made of block copolymers poly(ethylene oxide) (PEO) and poly(aspartic acid) loaded with the anticancer drug, adriamycin[4].

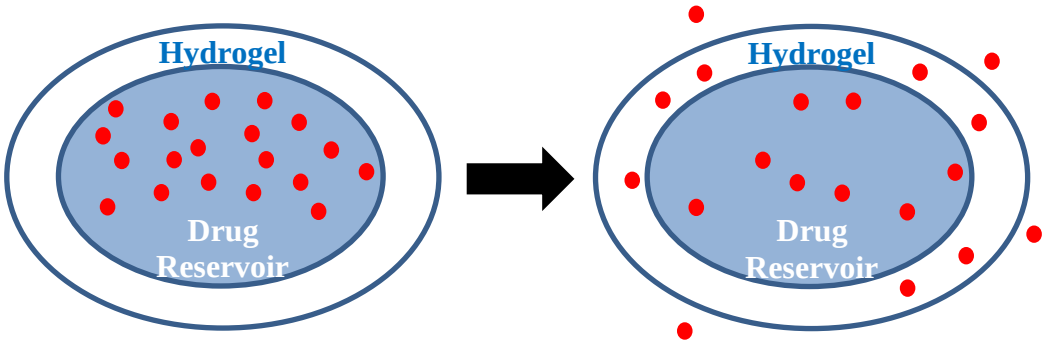


**Figure 1:** Illustration of hydrogels as drug delivery systems.
Hydrogels are loaded with drugs. As the drug-loaded hydrogel travels through the body, the drugs are protected from the harsh conditions until it reaches to targeted area where the drug can diffuse out of the pores of the hydrogel.

### 1.2.2 Tissue Engineering

Hydrogels have attracted considerable attention for tissue engineering and regenerative medicine applications (Figure 2). Tissue engineering requires cells to be cultured and maintained in suitable scaffolds under appropriate growth conditions. Hydrogels are an appealing option for this purpose because their structures mimic the extracellular matrix of many natural tissues. Skaalure and colleagues have encapsulated bovine chondrocytes in a newly developed, degradable PEG-based hydrogel that shows promising results for cartilage tissue engineering. This hydrogel successfully preserved the chondrocyte phenotype and promoted a hyaline-like engineered cartilage tissue[5].

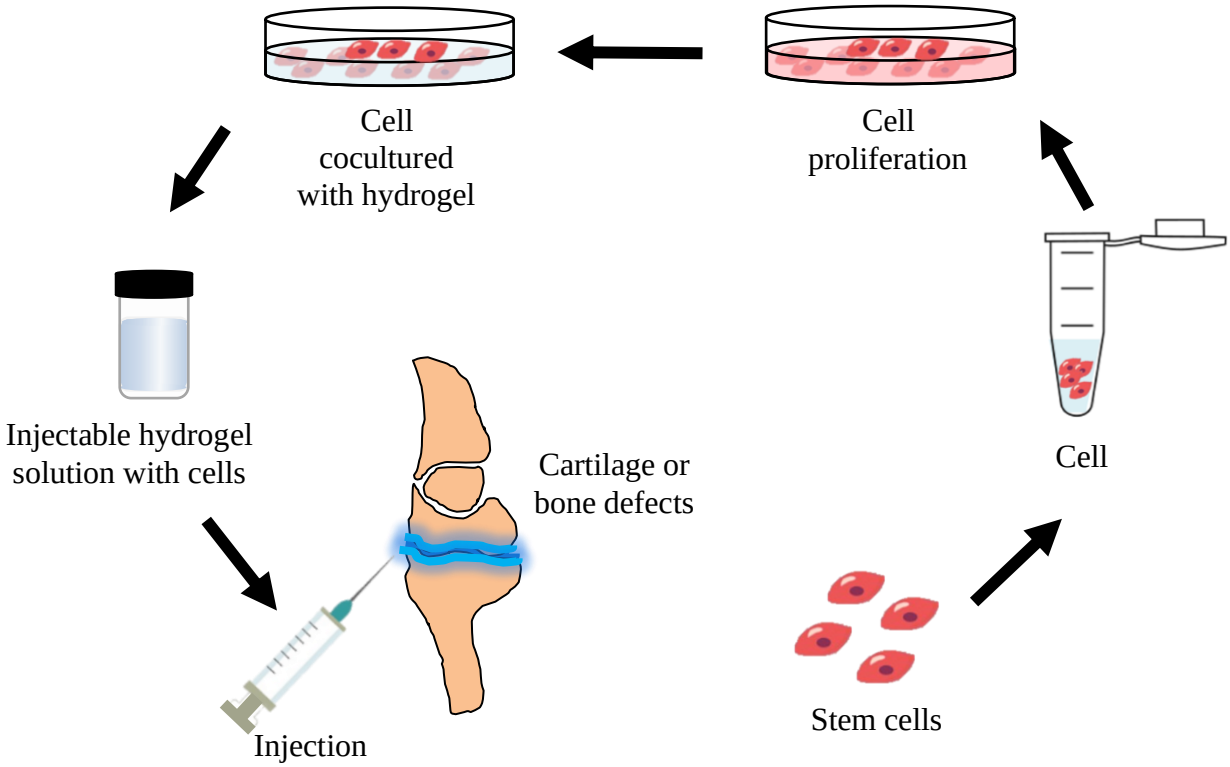


**Figure 2:** Role of hydrogels in tissue engineering.
Hydrogels act as a scaffold for culturing cells designed for regenerating cartilage or bone due to their close resemblance to the extra cellular matrix. The shear-thinning behavior is also used to form an injectable treatment for implanting cells into cartilage or bone defects.

### 1.2.3 Engineered Living Materials

Engineered living materials are a new technology that incorporates living microbial organisms within hydrogel matrices. Compared to traditional liquid cultures of living cells, both components in engineered living materials can be programmed to meet specific goals. The living cells can be engineered to fulfill a multitude of functions, ranging from sensing to chemical production, and even generation of electricity[6]. Hydrogels are a popular construct for these materials for a number of reasons. Most hydrogels offer a high degree of biocompatibility and chemical permeability that make it ideal for sustaining living microbes. The high water content associated with hydrogels also provides the necessary hydration for the encapsulated living cells. The hydrogel construct can also be designed to create chemical gradients, mechanical confinement, and spatial compartmentalization of living cells. A unique quality of engineered living hydrogels is their ability to interact with external stimuli. It is this quality that makes them a versatile tool in industry and biomedicine. The hydrogel matrix acts as a scaffold for maintaining cell viability, diffusion of chemicals in and out of the network, and light transmission. The encapsulated microbes perform biological functions in response to changes in environmental conditions. This coupled communication between engineered living hydrogels and the environment makes them an excellent candidate for use as sensors for diseases, treatments for environmental pollution, and batteries for electrical energy conversion. Typically, external signals, such as heat, light or chemicals, are delivered through the hydrogel network to the encapsulated microbes. Once that signal is received, the cells respond by generating outputs, such as fluorescence, bioluminescence, or conductivity in cells[6]. The ability for engineered living hydrogels to sense and respond to changes in the environment enable them to monitor metabolite production. For example, Courbet et. al genetically modified *E. coli* and *B. subtilis* and

successfully encapsulated them in PVA-alginate hydrogel beads. These bacterial sensors were genetically encoded with digital amplifying genetic switches that were able to detect pathological glycosuria in urine from diabetic patients[7].

## 1.3 Motivation and Objectives

Advances in Synthetic Biology (SynBio) are providing innovative means of addressing societal issues, such as sustainable manufacturing, resource scarcity, and access to responsibly produced goods and services[8]. SynBio is the incorporation of engineering practices to design new biological components, like cells, enzymes or genetic pathways, or to redesign existing biological systems. SynBio is distinguished from traditional molecular and cellular biology in that it's focus is on the design and manufacture of key biological components that can be engineered to meet specific performance criteria. The primary motivation behind the research presented in this thesis is to contribute to the collaborative effort amongst an interdisciplinary team of researchers funded by the National Science Foundation (NSF). This group consists of researchers from the University of Texas in Austin (The Alper Group) as well as several research groups from the University of Washington (the Carothers Group, the Nelson group, Machine Agency, and the Pozzo Research Group). This group is interested in expanding the potential of SynBio by developing next generation bioreactors capable of converting cheap raw materials (such as sugars and amino acids) into high-value products such as pharmaceuticals and chemical intermediates using yeast and bacteria as the biocatalysts. Current manufacturing processes for these chemicals of interest require sourcing materials that rely on unsustainable farming practices. For example, the production of artemisinin, an antimalaria drug derived from wormwood plants from Asia and Africa, requires large amounts of land to achieve necessary yields and an inefficient extraction process that generates large volumes of solvent waste.

Developments in SynBio could introduce a more sustainable option where semi-synthetic artemisinin is derived from genetically-modified yeast[9]. Unfortunately, measures to upscale this process have not yet been successful and further research is required. In addition to this, food production is yet another potential application that could benefit from SynBio. Meat consumption in the US has risen 40% since the 1960s[10]. Raising livestock to keep up with the increasing demand for meat, generates 15% of the total global greenhouse gas emissions. It also relies on 70% of agricultural land, which leads to deforestation, loss of diversity and pollution[11]. With SynBio, current unsustainable farming practices could be replaced with a more sustainable option where meat is grown from living tissue in bioreactors (Figure 3).

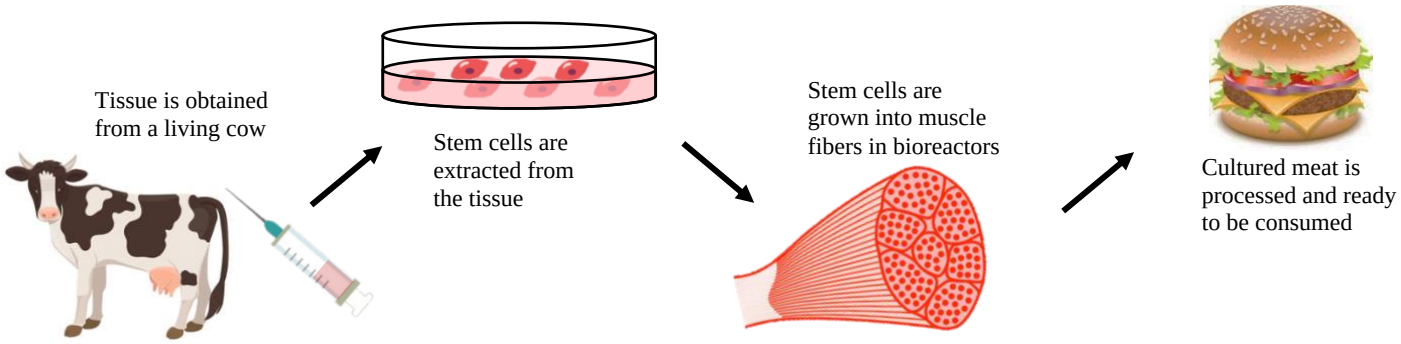


**Figure 3:** Example of SynBio as a solution for unsustainable farming practices. Stem cells are extracted from tissue from a living cow and grown into muscle fibers in bioreactors where they are processed into cultured meat.

This group hypothesizes that current technologies associated with distilleries, breweries, and biorefineries could be reimagined with modular reactor technologies to distribute products from low and medium-scale bio-manufacturing. The next generation bioreactors that are currently being developed rely on microbes encapsulated within a hydrogel network. These microbe-laden hydrogels are an ideal platform as they meet the design criteria required. The platform must be able to provide containment of the microbes but still allow the flow of materials, such as

substrates and products, in and out of the system. The platform must have a high degree of mechanical integrity to prevent cell leakage while also maintaining cell viability. These engineered living hydrogels would provide optimized transport of substrates into the suspended biocatalysts and the removal of products out of the gel frameworks for efficient downstream separation and purification (Figure 4). Researchers from the Nelson group have performed extensive research on cell viability within the hydrogel network; however, they have highlighted

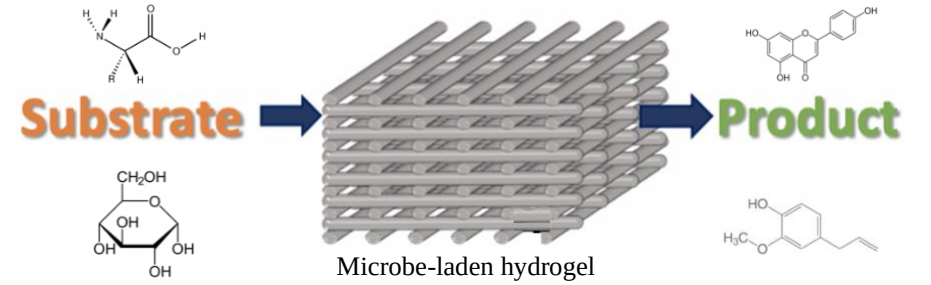


**Figure 4:** Illustration of the flow of substrates in and products out of the microbe-laden hydrogel.

the need for a comprehensive understanding of the cellular response within the hydrogels to better synthesize advanced living materials to meet the needs for specific applications[12]. Since a strong relationship exists between the mechanical and structural properties of hydrogels, it is imperative that the structural makeup of the hydrogel platform is understood[2]. Therefore, this thesis will focus on utilizing small angle X-ray scattering to probe the structure of Pluronic F127 through the process of functionalization, polymerization and lyophilization (i.e. freeze drying).

The research presented in this thesis aims to use small angle X-ray scattering to fulfill three main objectives. First, to determine if the process of functionalizing Pluronic F127 with bisurethane methacrylate (to form F127-BUM) introduces significant changes to the crystal structure that could ultimately affect the gelation and rheological properties of this polymer. Second, to probe the structure of F127-BUM hydrogels to determine if the free radical

polymerization process introduces defects within the hydrogel network that could adversely affect future downstream processing of compounds of interest. And finally, to examine the lyophilization and rehydration process of F127-BUM hydrogels to ensure the crystal structure is preserved.

# Chapter 2: Materials

## 2.1 Polyether Block Copolymers

Pluronics, also known as poloxamers, are tri-block copolymers consisting of hydrophilic poly(ethylene oxide) (PEO) end groups and a hydrophobic poly(propylene oxide) (PPO) middle group. Pluronics are represented by a formula consisting of three segments. The leading character indicates the physical form at room temperature ("L" for liquid, "P" for paste, "F" for flake). The second character indicates the length of the PPO block. Multiplying this value by 300 gives the approximate molecular weight of the PPO center block. The final digit indicates the mass fraction, as 1/10$^{th}$ the weight percentage, of the PEO end groups[13]. Figure 5 represents a graph summarizing a number of commercially available Pluronics organized from increasing PPO molecular weight along the y-axis and increasing PEO weight percent on the x-axis[14]. F127 was selected for its relatively high solubility in water (due to the PEO side groups) and for its interesting thermo-reversible gelation properties. It also has the ability to self-assemble in aqueous media without additives.

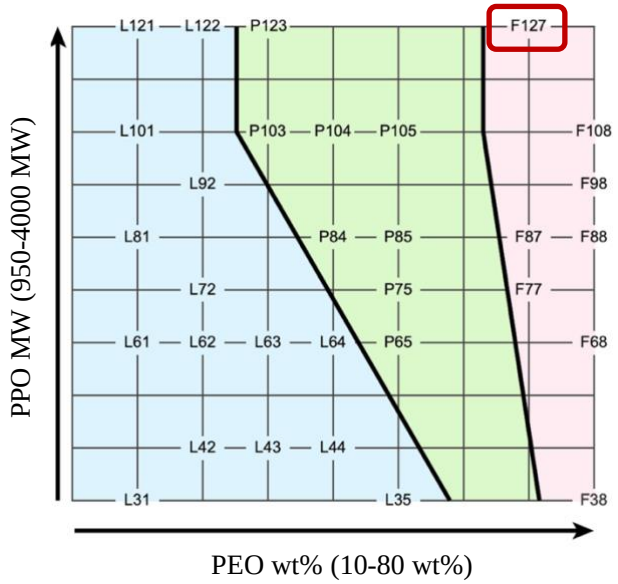


**Figure 5:** Graphic illustrating all of the commercially available Pluronics. Pluronics grid is organized by increasing PPO and PEO groups[14].

The high PEO composition contributes to a high solubility and stability in aqueous solutions. They are widely used as cosmetics, foaming agents, and emulsifiers. They have also been widely explored as drug delivery systems as well as pharmaceutical carriers due to their low toxicity and unique temperature-sensitive gelation behavior.

When block copolymers, like Pluronic F127, are mixed with water, self-assembly, also known as micellization, can be achieved by varying the temperature for a given concentration, or by varying the concentration at a given temperature[15]. A schematic of this process is represented in Figure 6[16].

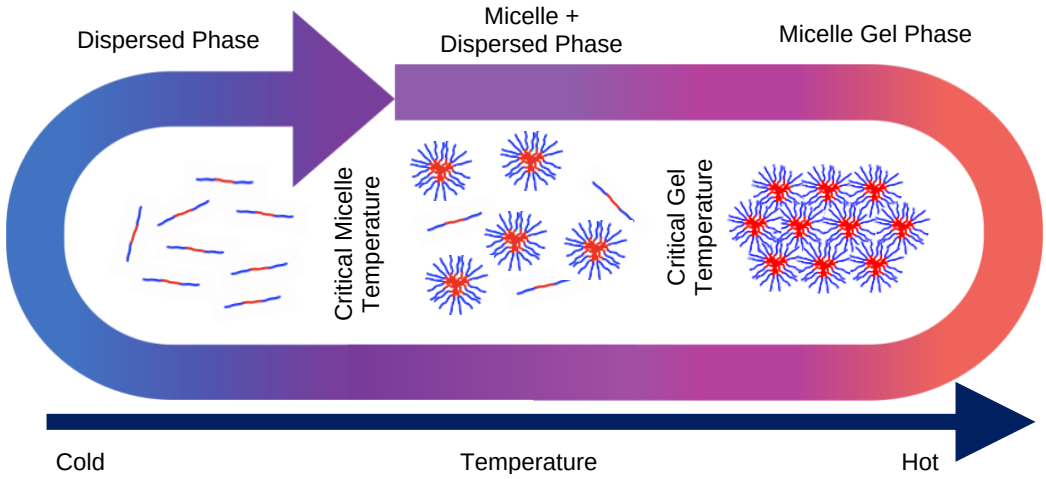


**Figure 6:** The temperature-dependent micellization and gelation of Pluronic polymers[16]. At low temperatures, both PPO and PEO groups are soluble in water and form a dispersed phase. As temperatures increase, the solubility of PPO decreases and micelles begin to form at the critical micelle temperature. As temperatures continue to increase, even more micelles form and the critical gel temperature is reached. As the number of micelles increase, repulsive interactions get stronger and micelles begin to order into quasi-crystalline cubic lattices.

When first exposed to solution at low enough temperatures, both the PPO and PEO groups are soluble in water forming a dispersed phase. As the temperature increases, the solubility of the PPO center group decreases and micelles begin to form to avoid contact between the water and the PPO hydrophobic section. The solution crosses a point (known as the critical micelle

temperature, or CMT) where an equilibrium balance of dispersed polymer chains and newly formed micelles is achieved. A natural phenomenon known as the hydrophobic effect is the entropic driving force of micellization. Hydrophobic molecules (specifically the PPO section of the Pluronic) associates with one another to dissipate the "water cages" of ordered water molecules that form around each hydrophobic molecule[17]. As the temperature continues to increase, more and more micelles form. The growing number of micelles experience repulsive interactions and begin to order into quasi-crystalline cubic lattices.

This self-assembly behavior gives rise to several unique phase behaviors, such as the formation of micelles of various shapes and sizes, complex structured microemulsions, and liquid-crystalline phases. Extensive research has been conducted to not only understand the formation of micelles and the structure of the resulting Pluronic hydrogels, but also various systems containing Pluronics to determine the effect on micellization and gelation. McConnell and Gast demonstrated that the formation of BCC and FCC/HCP structures below the order-disorder transition depended on the micellar corona thickness. They concluded micelles with thinner coronas favored an FCC structure due to their greater short-range inter-micellar repulsions and thicker coronas favored BCC ordering due to soft interaction potential[18]. Hamley et al. identified regions of temperature-induced order-order transition caused by the degree of hydrophilicity of PEO and PPO systems via SAXS. They reported BCC phase for low-temperature systems at concentrations greater than 30 wt% copolymer and FCC structure for all other conditions. They attributed the BCC phase at high copolymer concentrations to the increasing softness associated with the interactions between spheres as the concentration of copolymer increases[19]. Despite all of the research that has been conducted on F127 systems, there is still disagreement on the true nature of the structures formed. Mortensen and colleagues

observed two-dimensional neutron scattering patterns of a shear-aligned sample of F127 micelles and determined a BCC-ordered micellar phase occurs in 20 wt% F127 solution. This conclusion was based on identical scattering patterns that were previously observed in P85 and F88 copolymers where extensive crystallographic studies were used to validate the results[20]. These results were also supported by a study conducted by Prud'homme et al[21]. Conflicting results were reported by Wu et al., who reported on X-ray scattering data that suggested the formation of an FCC structure rather than BCC[22]. Mortensen and colleagues explored the source of this disagreement and used SAXS to determine that both conclusions regarding BCC and FCC lattices could in fact be true. They published results suggesting that the concentration of di-block copolymer PPO-PEO impurities in commercial block copolymers of PEO-PPO-PEO influenced the phase behavior. F127 solutions containing 20% of the di-block copolymer consistently showed FCC-ordered structure within the gel phase. In purified F127 samples free of di-block copolymer, the samples demonstrated BCC arrangement in the major parts of the gel phase. However, as the system approached the disorder to order transition, FCC structures were observed[23].

## 2.2 Current Applications of Pluronic F127

Because Pluronic F127 exhibits gelation near body temperatures for polymer concentrations between 15-30 wt% and it has been approved by the FDA due to its low toxicity, it is one of the most widely used Pluronics in biomedicine. Many studies have shown that F127 can self-assemble into spherical micelles when dissolved in solution. These micelles assume a core-shell structure, where the core is dominated by the hydrophobic PPO blocks, while the corona, which is in contact with the aqueous environment, is comprised of hydrophilic PEO

blocks. The unique structural characteristics of Pluronic F127 make it an ideal candidate for a wide variety of applications.

The high accessibility and bioavailability of dental-derived mesenchymal stem cells (MSCs) are an excellent therapeutic candidate for tissue engineering; however, maintaining adequate survival rates of the cells while delivering MSCs to the appropriate defect site is still a hurdle that researchers must overcome. Diniz and colleagues successfully used Pluronic F127 as the hydrogel scaffold to encapsulate dental pulp stem cells (DPSCs) in vitro. They were able to achieve high stem cell viability and proliferation which suggests immobilization of DPSCs in Pluronic F127 hydrogels is a viable strategy for tissue engineering[24].

Cidade et al. developed a hydrogel using Pluronic F127 as the continuous phase and alginate microparticles as the dispersed phase of the system. They took advantage of the unique thermoresponsive property of Pluronic F127 to load the hydrogel with a model drug and inject while in its sol state. Methylene blue was used as the model drug to perform release studies in methylene blue loaded Pluronic hydrogel as well as methylene blue loaded alginate microparticles and Pluronic hydrogel composite system. The composite system demonstrated a slower methylene blue release. This illustrates the potential of Pluronic F127 as the vehicle for a dual cargo release system for drug delivery[25].

Nelson and colleagues also took advantage of the unique properties of F127 and developed an extrudable, shear-thinning hydrogel ink[26]. Extrudability of the hydrogel means that many unique shapes can be printed to meet the needs of any situation. Once cured, stretchable hydrogels could be created with a wide array of potential applications ranging from tissue engineering, implantable devices and bioreactors. They determined functionalizing F127 with bisurethane methacrylate would help overcome a significant challenge: to develop hydrogels that

can be easily processed into the desired form factor form of F127 while also achieving the right physical and biochemical properties. Therefore, they developed the functionalized form of F127 known as F127-BUM that could be photo-cured to permanently hold its form but would not result in significant changes to the mechanical properties. They leveraged this material to immobilize *S. cerevisiae* within the hydrogel network, thus forming an engineered living material (ELM). Although they were able to successfully maintain cell growth within the hydrogel, they also observed degradation of the polymers likely due to the cellular inhabitants. The group's research highlighted the need for a comprehensive understanding of the cellular response within the hydrogels to better synthesize advanced living materials to meet the needs for specific applications[26].

## 2.3 Hydrogel Preparation

F127 neat and the photoinitiator (2-hydroxy-2-methylpropiophenone) were purchased from Sigma-Aldrich and the functionalized form of F127-BUM was made and provided by the Nelson Research Group. The preparation of F127 neat hydrogels is outlined in Figure 7 below.

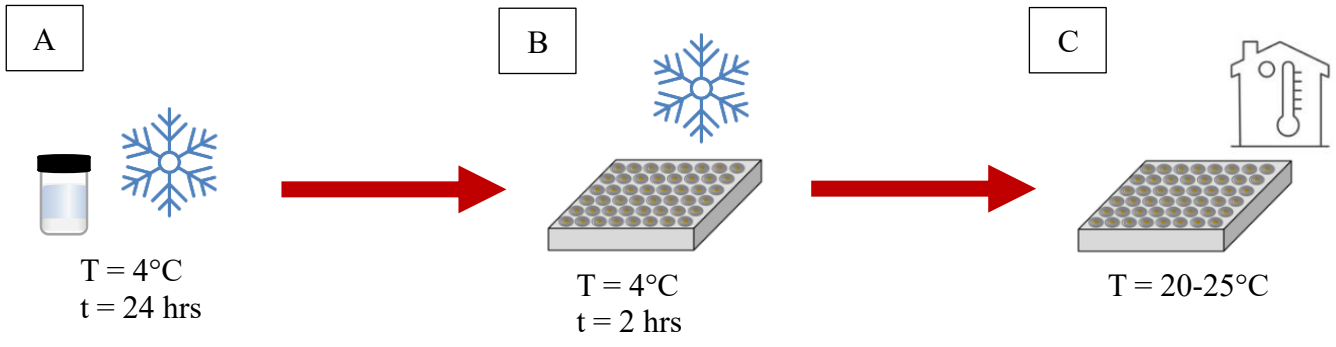


**Figure 7:** Sample preparation for F127 neat hydrogels.
A) F127 neat and cold deionized water is added to a scintillation vial and left in the refrigerator overnight to fully dissolve. B) Once the polymer is fully dissolved, the solution is poured directly into the SAXS sample cartridge. The cartridge is placed back in the refrigerator to return to the sol state to uniformly fill the well. C)The cartridge is removed and left at room temperature to fully gel.

The appropriate amount of F127 neat to achieve the desired weight concentration was added to a scintillation vial and then cold deionized water was added. The solution was left in the refrigerator overnight to fully dissolve (Figure 7-A). Once the gel was fully dissolved, the solution was poured directly into the sample cartridge used for small angle X-ray scattering. The cartridge was placed in the refrigerator to allow the hydrogel to return to its sol state to uniformly fill the wells (Figure 7-B). After two hours in the refrigerator, the sample cartridge was removed and left at room temperature to achieve the final gel state (Figure 7-C)

F127-BUM hydrogels were prepared in a similar way (Figure 8). The Nelson group made F127-BUM by functionalizing the end groups of F127 through the activation of the alcohol group and a tin catalyzed isocyanate coupling reaction[26]. To make the gel, the appropriate amount of F127-BUM to achieve the desired weight concentration was added to a scintillation vial and then cold deionized water was added. The solution was left in the refrigerator overnight to fully dissolve (Figure 8-A). Once the F127-BUM was fully dissolved, the photoinitiator (PI) was added at a 1:1 ratio of grams of hydrogel to microliters of PI (Figure 8-B). The vial was wrapped in foil and placed back in the refrigerator for at least 24 hours to allow the PI to fully incorporate into the solution (Figure 8-C). The hydrogel solution was then poured into a small Petri dish, covered with foil, and placed back in the refrigerator for 2 hours to return to its sol state to achieve even spreading of the gel within the dish (Figure 8-D). The covered dish was then removed from the refrigerator and left out at room temperature to fully gel (Figure 8-E). After gelation was achieved, the foil was removed and the hydrogel was exposed to UV light for 20 minutes to initiate polymerization (Figure 8-F). A cork borer was then used to punch out small, uniform samples from the cured hydrogel (Figure 8-G).

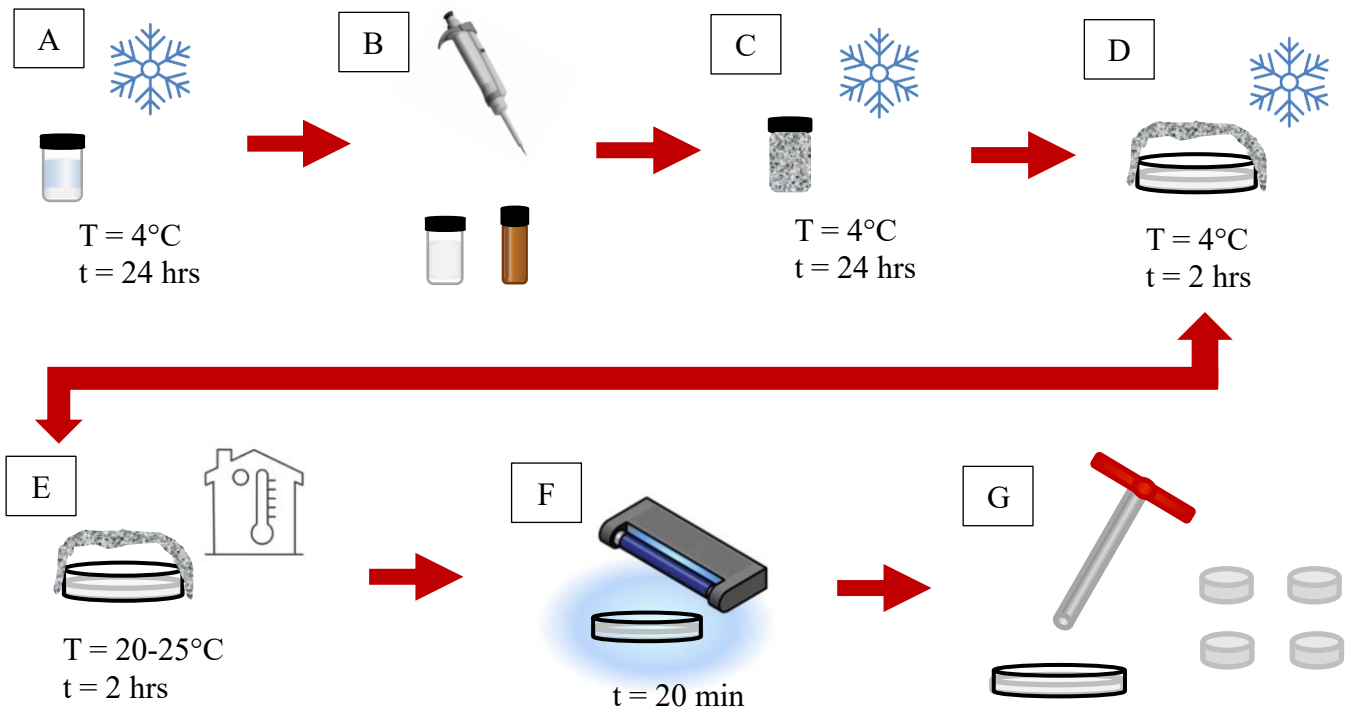


**Figure 8:** Sample preparation for F127-BUM hydrogels.
A) F127-BUM and cold deionized water are added to a scintillation vial left in the refrigerator overnight to fully dissolve. B) Once the F127-BUM was fully dissolved, the photoinitiator (PI) was added at a 1:1 ratio of grams of hydrogel to microliters of PI. C) The vial was wrapped in foil and placed back in the refrigerator overnight allow the PI to fully incorporate into the solution. D) The hydrogel solution is poured into a small Petri dish, covered with foil, and placed back in the refrigerator for 2 hours to return to its sol state for even spreading of the gel within the dish. E) The covered dish is removed from the refrigerator and left out at room temperature to fully gel. F) After gelation was achieved, the foil was removed and the hydrogel was exposed to UV light for 20 minutes to initiate polymerization. G) A cork borer is used to punch out small, uniform samples from the cured hydrogel.

# Chapter 3: Experimental Methods: Small Angle X-ray Scattering

## 3.1 Introduction to the Technique

Small angle scattering (SAS) is a non-destructive technique used for probing the structure of samples in solution. The primary benefit to this technique is its ability to investigate a sample structure in-situ over a wide range of length scales. Small angle scattering from light, X-rays and neutrons are analogous techniques that can successfully probe a variety of components of a sample. The research presented in this investigation will focus on small angle X-ray scattering (SAXS). The following sections are presented to provide the necessary information to interpret the X-ray scattering results presented in subsequent sections within this thesis.

The setup of a SAXS experiment is conceptually simple and is outlined in Figure 9[27].

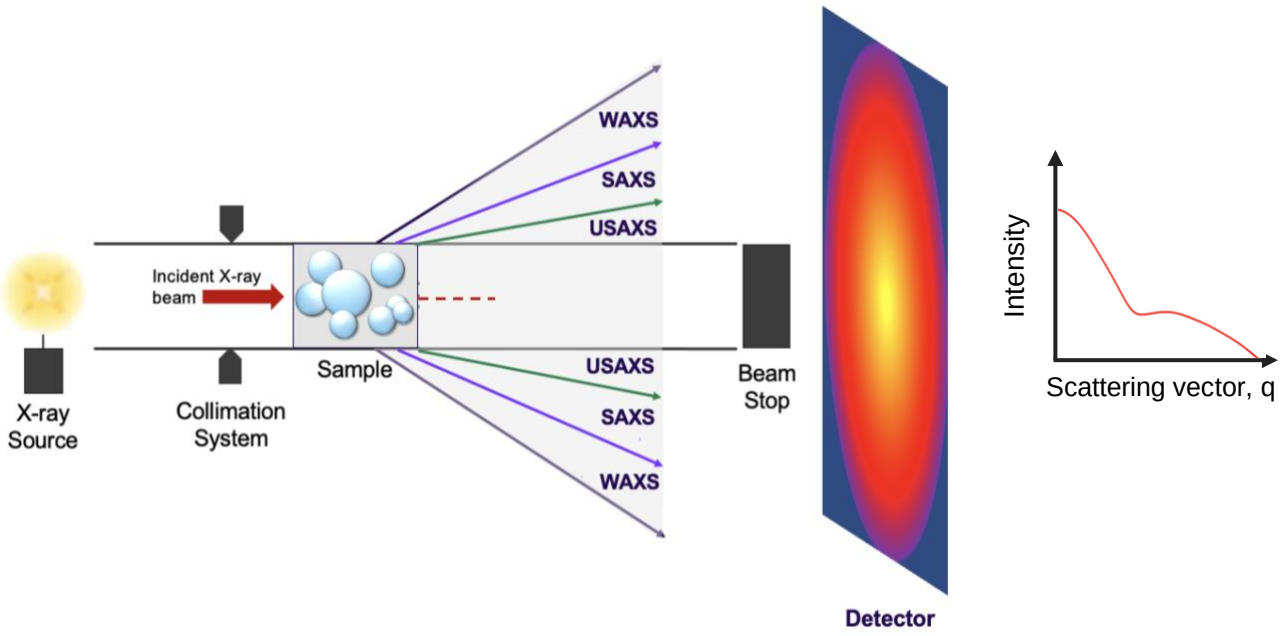


**Figure 9:** Basic illustration of small angle X-ray scattering experiment[27].
First, X-rays are generated from a source and pass through a collimation system to eliminate diverging beams. The beams irradiate the same. The X-rays scatter off the sample at different angles where they eventually hit the detector where they are recorded. The scattering pattern is radially averaged and integrated along the angle resulting in a one-dimensional curve of intensity as a function of scattering vector, *q*.

X-rays are generated from a source and passed through a collimation system to eliminate diverging beams. The beams exit the collimator where they irradiate the sample. When the X-ray beam contacts the sample, some of the X-rays are transmitted and others are scattered. In SAXS, the interactions that occur between the sample and the beam are considered elastic, in which no energy is transferred between the sample and the beam. The X-rays scatter off the sample at different angles where they eventually hit the detector where they are recorded[27]. The scattering pattern of the particles in solution is isotropic since they are arranged in a random orientation. Since a two-dimensional detector is typically used, the scattering pattern can be radially averaged and integrated along the angle resulting in a one-dimensional curve of intensity as a function of scattering vector, $q$. The scattering pattern of the pure solvent is collected as well and subtracted from the sample solution's scattering profile leaving only the signal from the particles of interest. The resulting scattering pattern is related to the overall shape and size of the particles being investigated. Because scattering is an inverse technique, $q$ has units of reciprocal length, typically $Å^{-1}$. Therefore, features observed at low $q$-values represent larger length scales and features observed at high $q$-values represent smaller distances[28].

When using scattering techniques to investigate particles in solution, the scattering pattern depends on the three-dimensional structure of the scattering objects and the distance between them. Specifically relating to the use of X-rays as incident radiation, which is the focus of this thesis, the scattering occurs with the electrons within the sample. Therefore, samples with higher electron-density will scatter with higher intensity than samples containing lower electron densities[28]. The scattering length density (SLD), $\rho$, is used to quantify the difference in scattering contrast between volume elements, and it is defined as the ratio of the scattering length per molecule and its molecular volume. Equation 1 provides the SLD for an $A_mB_n$ molecule where $b$

is the coherent scattering length of the atoms, *v* is the volume that is occupied by the molecule, and *m* and *n* are the number of each atom in the molecule[28].

$$\rho_{A_mB_n} = \frac{mb_A + nb_B}{v} \quad (1)$$

Characteristic distances between the electrons will produce scattering signals at different scattering angles. Therefore, probing the intensity of the scattering signal at different angles gives insight into distinct length scales (Figure 10). Large structures, such as microbes, give rise to scattering at very small angles and can be probed using ultra small angle X-ray scattering (USAXS). Much smaller structures, such as segment length of polymers, micelles and even colloids, can be probed using small angle or wide angle X-ray scattering (WAXS). The smaller the angle, the more difficult it becomes to separate the weak scattered intensity from the strong main beam source[30]. This is similar to observing a weakly radiant object close to the sun. The sun's radiation is so bright that it is impossible to observe its corona. During a solar eclipse, when the moon passes between the Earth and the sun, the intense radiation from the sun is blocked and the corona can finally be observed. Similarly, with SAXS, the non-scattered X-rays that pass through the sample must be blocked without blocking the closely adjacent scattered X-rays. Most X-ray sources produce divergent beams which compounds this complication. Performing SAXS measurements on a synchrotron source helps to overcome this issue since they use large bent mirrors to focus the beam[30].

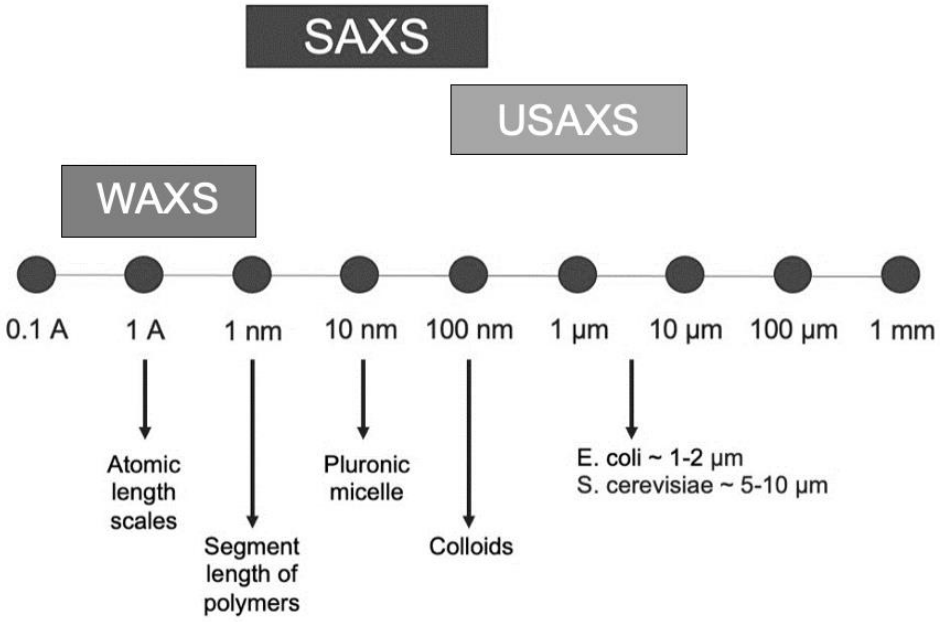


**Figure 10:** Range of length scales probed by small angle X-ray scattering.

## 3.2 Fundamental SAXS Principles and Equations

The scattering intensity of a simple system containing two components can be modeled as the self-correlation of discrete entities. These discrete entities can be particles or micelles. The self-correlation function is usually divided into terms that account for the contribution from both the individual particle's shape and size, as well as contributions from the arrangement of the particles within the sample. This is represented by Equation 2 below:

$$I(q) = NV_p^2 \Delta\rho^2 P(q) S(q) + background \qquad (2)$$

where *N* is the number density of the particles, $V_p$ is the volume of a single particle, $\Delta\rho^2$ represents the contrast factor, *P(q)* is the single particle form factor and *S(q)* is the interparticle structure factor, and the background is from incoherent scattering intensity[29].

The form factor, $P(q)$, accounts for the scattering that results from one particle. Since all of the atoms within the particle will result in a scattering wave, all of the wave amplitudes are

summed. This results in a unique interference pattern that provides insight into the shape of the particle based on its unique oscillation[30]. Particle form factors can be determined experimentally if extremely dilute conditions are achieved and if the particles shape does not change with concentration. At very dilute concentrations, the spatial correlations between particles are considered negligible and the structure factor effectively goes to 1 for all $q$[29]. Unfortunately, it is not possible to use this method for micelles because their shape will change with concentration and they cannot be diluted to measure *P(q).* Therefore, knowledge of the system is needed to assume an appropriate geometry for calculating the form factor. Equation 3 can be used to mathematically calculate the form factor, $P(q)$, which is the density correlation function integrated over the particle volume:

$$P(q) = \left[\frac{1}{V_P}\int_{V_P} e^{iqr}dr\right]^2 \quad (3)$$

The monodispersed sphere is the simplest particle geometry. Assuming a uniform density, the form factor for this simple geometry, represented by $P_{sphere}(q)$ is given by Equation 4, where $R$ is the particle radius[31]:

$$P_{sphere}(q) = 9\left[\frac{\sin(qR) - qR\cos(qR)}{(qR)^3}\right]^2 \quad (4)$$

For a system represented by polydispersed spheres, the form factor is a weighted sum based on the size distribution of the particles.

The core-shell model is also an appropriate geometry to assume for spherical micelles. The form factor for this geometry is given by Equation 5 and all relevant variables are shown in Figure 11[32]:

$$P_{core-shell}(q) = 9\left[\frac{V_c(\rho_c - \rho_{solv})\sin(qR_c) - qR_c\cos(qR_c)}{(qR_c)^3} + \frac{V_s(\rho_s - \rho_{solv})\sin(qR_s) - qR_s\cos(qR_s)}{(qR_s)^3}\right]^2 \quad (5)$$

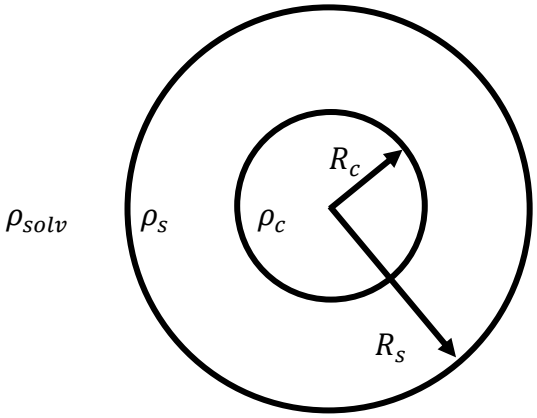


**Figure 11:** Representation of the relevant variables of the core-shell model. $R_C$ represents the radius of the core and $R_S$ represents the radius and thickness of the entire particle. $\rho_{solv}, \rho_s$, and $\rho_c$ represent the scattering length density of the solvent, shell, and core, respectively.

If the particles in a sample are ordered in a crystalline arrangement, correlation peaks will form. These peaks are the result of highly ordered samples with interference patterns combining constructively. Crystals formed from different lattices will result in diffraction peaks with different relative spacing. The relative peak spacing for common crystal lattices is summarized in Table 1.

**Table 1:** Bragg's Peak Positions for Common Crystal Lattices

| Structure | | Ratio q/q* |
|---|---|---|
| FCC | 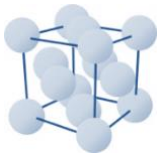 | $1, \sqrt{4/3}, \sqrt{8/3}, \sqrt{11/3}, \sqrt{12/3}, \sqrt{16/3}, \ldots$ |
| BCC |  | $1, \sqrt{2}, \sqrt{3}, \sqrt{4}, \sqrt{5}, \sqrt{6}, \ldots$ |
| HCP | 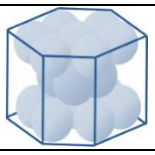 | 1, 1.06, 1.13, 1.46, 1.73, 2.56, … |
| HEX |  | $1, \sqrt{3}, \sqrt{4}, \sqrt{7}, \sqrt{9}, \sqrt{12}, \ldots$ |

The spacing within the crystalline arrangement, $d$, can be approximated using the location of the correlation peak, $q_{peak}$, with the following equation:

$$d = \frac{2\pi}{q_{peak}} \qquad (6)$$

The structure factor, $S(q)$, represents scattering due to interactions between particles. A structure factor occurs if the particles within a system are concentrated or if they assemble within close proximity to one another. Two isotropic structure factors that are most appropriate for approximating the interactions between micelles within the hydrogel systems described in this thesis include the hard-sphere fluid model (which describes particle fluids) and the paracrystal model (which describes crystalline solids)[29]. An illustration representing the scope of both of these models is presented in Figure 12. The paracrystal model starts with the assumption of a perfect crystal lattice and is capable of representing the degree of distortion of the position of the particles within the crystal as the system experiences disorder. This model is therefore able to

capture lattice defects that may occur within a crystal structure. When the specific cubic lattice is known, the two parameters that are adjustable are the dimension of the unit cell ( $a$ ) and the distortion parameter ( $g$ ). The hard-sphere model starts with the assumption of a dilute gas and can represent the spatial interactions that occur as the system becomes more concentrated. The only parameters that are adjustable within this model are the volume fraction ($\phi$) and the hard-sphere diameter ( $D$ ). It is worth noting that as the hard-sphere model becomes more concentrated and the paracrystal model becomes more disorganized, their structural description becomes more similar[29,33].

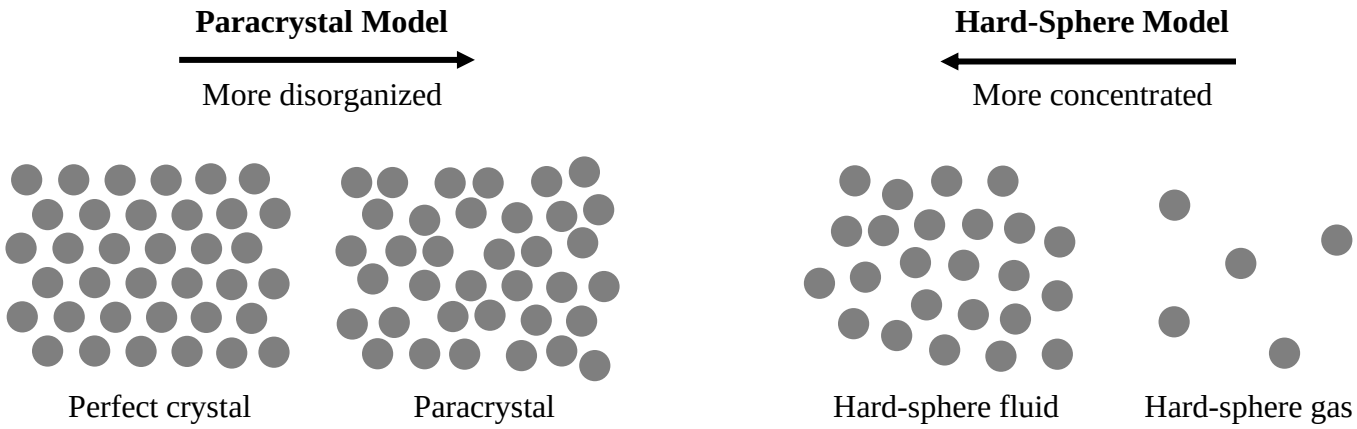


**Figure 12:** Graphical representation of the scope of the paracrystal model and the hard-sphere fluid model.

## 3.3 Experimental Setup

Small-angle X-ray scattering (SAXS) was performed on beamline 12-ID-C at the Advanced Photon Source at Argonne National Laboratory over a $q$-range of 0.01 to 1.3 $Å^{-1}$ in a pinhole configuration. The instrument used an X-ray source of 20 keV, corresponding to a wavelength of 0.62 Å, a beam size of 0.4 mm x 0.15 mm and a flux density of approximately 2 X $10^{12}$ photons/s/$mm^2$. Samples were loaded into a custom aluminum 48-well plate, sealed

between two Kapton windows[34] (Figure 13). SAXS data were collected at room temperature and with exposure times of 1 second each. Scattering profiles were radially integrated on-site using locally authored MATLAB software and were normalized using Kapton background subtraction.

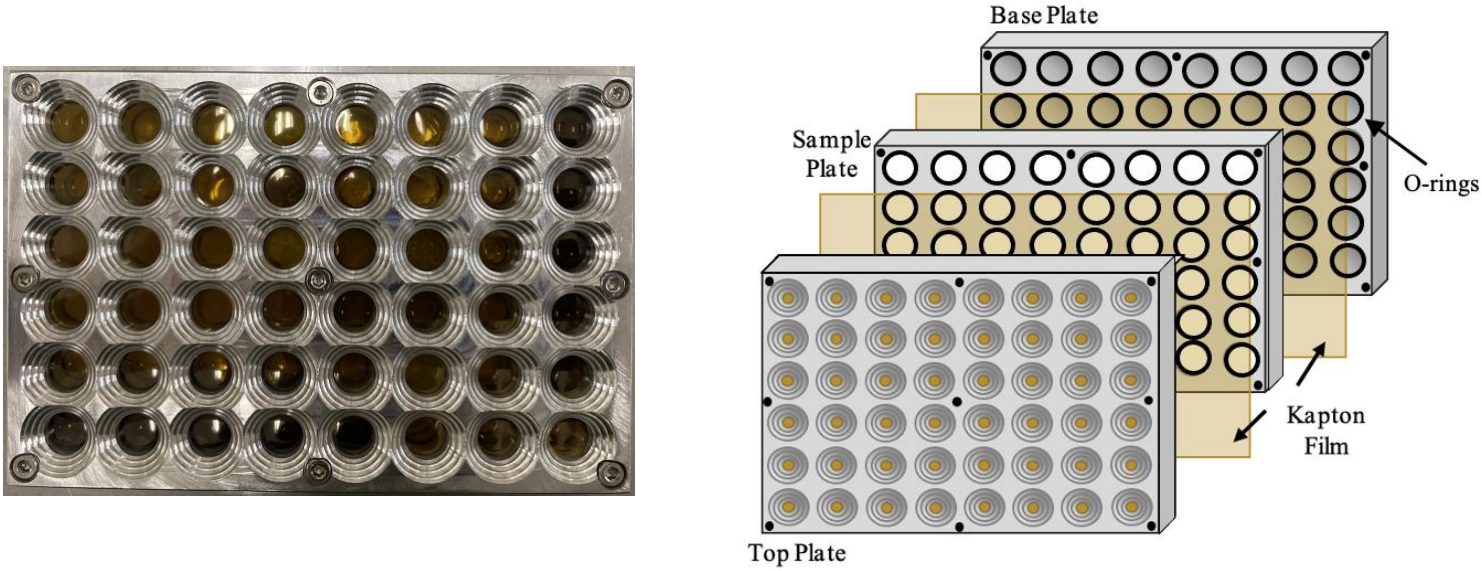


**Figure 13:** Custom aluminum 48-well plate used for SAXS measurements.

# Chapter 4: Results and Discussion

## 4.1 Functionalization of Pluronic F127 with Bisurethane Methacrylate

Hydrogels have gained considerable attention for a wide range of biomedical and industrial applications. Hydrogels based on synthetic polymers, such as Pluronic F127, are particularly attractive due to their unique response to changes in temperature, biocompatibility, and ability to retain large amounts of water. When considering an appropriate platform for a bioreactor, a hydrogel made from Pluronic F127 is an ideal candidate due to its ability to self-assemble in aqueous solutions. The resulting polymeric network is large enough for molecules of interest to diffuse through, but small enough that larger microbes will remain contained. The issue with developing bioreactors from Pluronic F127 is this platform is not protected from dissolution in water or media. Members of the Nelson group at the University of Washington have developed a functionalized form known as F127-BUM to address this issue. Pluronic F127 was functionalized at the chain-end through the activation of the alcohol group through a tin catalyzed isocyanate coupling reaction[26] (Figure 14).

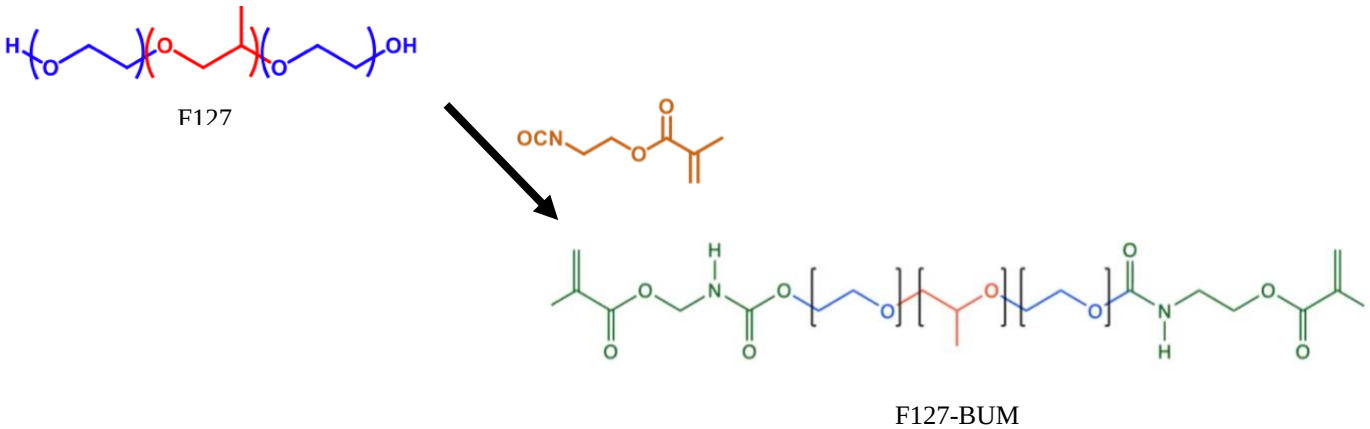


**Figure 14:** Synthesis of F127-BUM through the activation of the alcohol via tin catalyzed isocyanate coupling reaction.

The resulting polymer, containing bisurethane methacrylate end groups, can form cross-linked networks that will not dissolve when exposed to an excess of solvent (Figure 15).

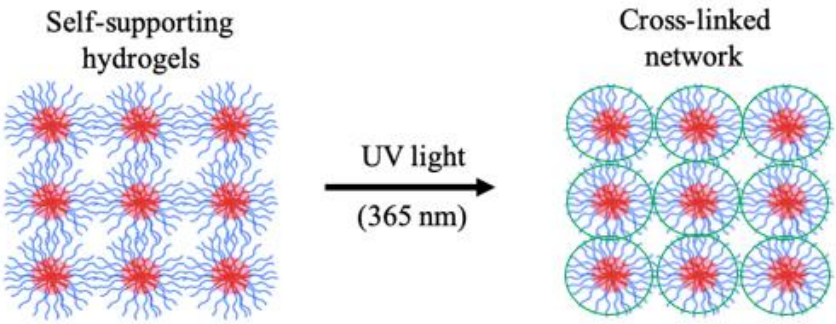


**Figure 15:** Functionalized F127-BUM forming cross-linked networks after exposure to UV light.

Extensive research has been conducted on F127 hydrogels over the last several decades. F127 can form hydrogels at 20-30 wt% and has a gelation temperature ($T_{gel}$) between 15 and 20°C. With the inclusion of the bisurethane methacrylate end groups, it was important to understand how this would affect the assembly behavior and rheological properties. Figure 16 shows phase diagrams for both neat F127 and F127-BUM at varying temperatures and weight concentrations[35]. The red boxes represent the weight concentrations of interest at approximately room temperature (between 20-25°C). At 25°C, all weight concentrations between 20-30% form transparent gels. At 20°C, all gels (with the exception of 20wt%) form transparent gels. F127 neat at 20°C and a weight concentration of 20% forms a transparent viscous solution whereas F127-BUM at the same conditions forms a transparent liquid. This suggests that functionalizing with bisurethane methacrylate has almost no effect on the gelation properties of the polymer.

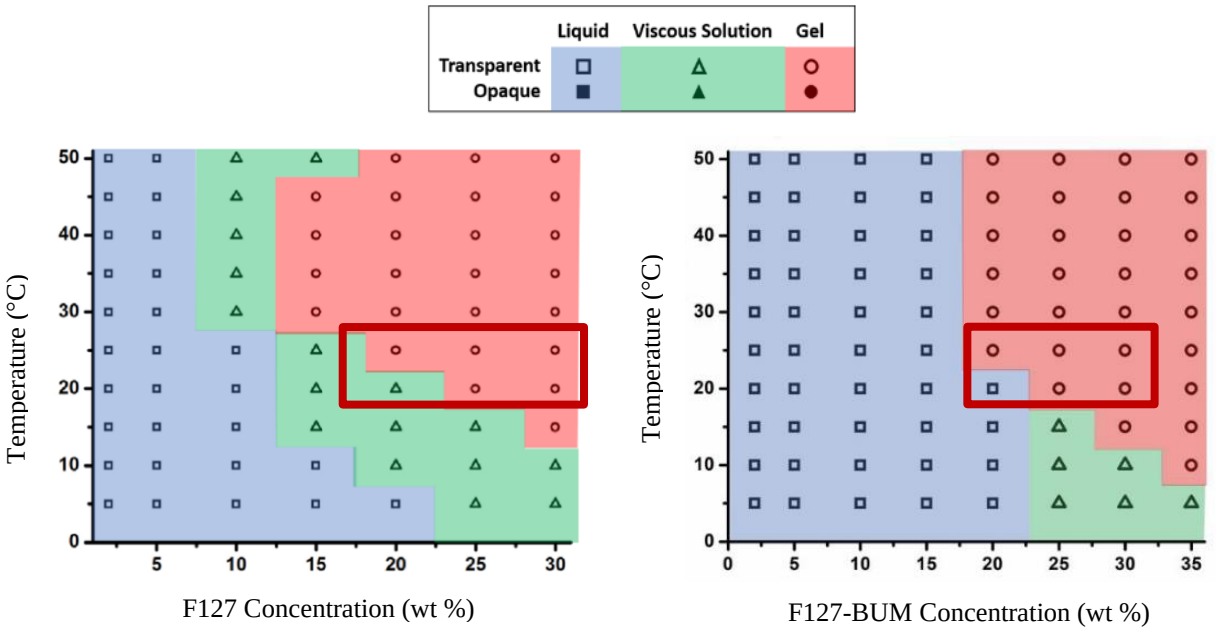


**Figure 16:** Phase diagrams of F127 and F127-BUM in water at various temperatures (0-50°C) and weight concentrations (0-30 wt% for F127 and 0-35 wt% for F127-BUM)[35].

Figure 17 shows yield stress and viscosity comparisons between the two polymers at 30 wt%[35]. For lower shear rates, the F127 gels have a slightly higher viscosity and for higher shear rates, the F127-BUM gel has a slightly higher viscosity. However, the differences between these values are considered negligible.

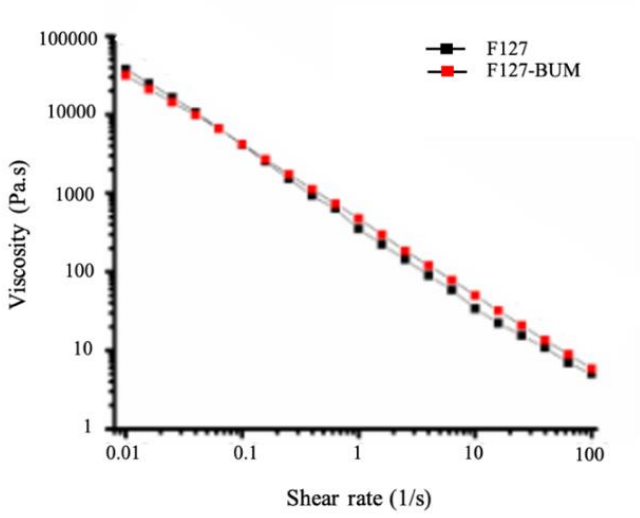


**Figure 17:** Rheology data for 30 wt% F127 and F127-BUM[35].

Both of these diagrams reveal that the chain-end functionalization had very little effect on the gelation behavior and rheological properties of F127.

Once the Nelson group determined there were no significant changes to the gelling behavior and rheology with the addition of the bisurethane methacrylate end groups, it was important to investigate the morphology of F127-BUM hydrogels using small angle X-ray scattering. The circularly averaged scattering profiles for both neat Pluronic F127 gels as well as the functionalized form of F127-BUM for polymer concentrations between 20-30 wt% are shown in Figure 18.

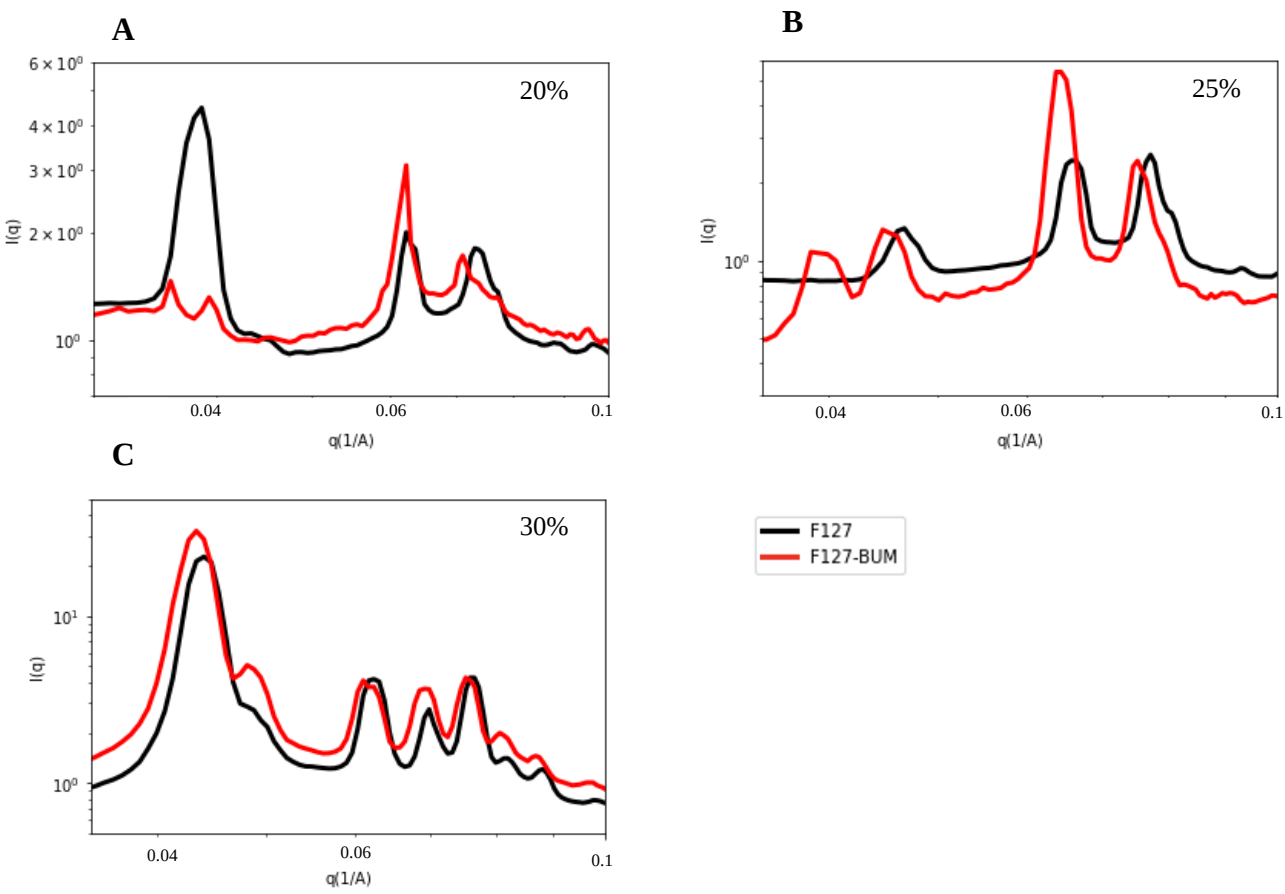


**Figure 18:** X-ray scattering profiles for neat Pluronic F127 gels versus functionalized F127-BUM gels at A) 20 wt%, B) 25 wt%, and C) 30 wt%.

Each of the profiles shows two peaks and a broad shoulder that are characteristic of face centered cubic (FCC) crystals, with the exception of 25 wt%. In the scattering profile for 25 wt%, the first peak appears to be missing. As was previously discussed in the SAXS section of this thesis, a SAXS curve consists of two factors: the form factor which contains information pertaining to the size and shape of the single particles and the structure factor which accounts for the interactions between neighboring particles. The visibility of a specific Bragg peak, such as the first one that is not visible in the scattering profile of 25 wt% F127, may be low if it appears close to a form factor minimum[30].

Using principles of crystallography, the missing first peak can be estimated. Crystals formed from different lattices will result in diffraction peaks with different relative spacing. Crystals containing cubic orientation have Bragg peaks as defined by Equation 7, where $a$ is the size of the unit cell and {h k l} represent the Miller indexes, a convenient way to mathematically represent a family of planes within a crystal[36].

$$q_{peak} = \frac{2\pi}{a}\sqrt{h^2 + k^2 + l^2} \quad (7)$$

The ratio of any known peak to the first diffraction peak is defined by Equation 8 and can be used to solve for an unknown peak:

$$\frac{q_i}{q_1} = \frac{\sqrt{h_i^2 + k_i^2 + l_i^2}}{\sqrt{h_1^2 + k_1^2 + l_1^2}} \quad (8)$$

For the face centered cubic lattice, the Miller indices for the planes corresponding the first two diffraction peaks are {111} and {002}[36]. Using Equation 8 and the known $q$ value for the second peak, the first peak for the 25 wt% scattering profile is estimated to be 0.04114 $A^{-1}$.

The position of the first peak for all other neat samples (in black) show a gradual shift to higher $q$ values as the concentration of polymer is increased. This shift suggests that the unit cell of the cubic crystal is smaller for the higher polymer concentrations. This is consistent with interactions between hard spheres. The concentration of polymer micelles increases as the concentration of polymer is increased. As a result, the micelles are pushed closer and closer together resulting in a crystal with a smaller lattice. A similar shift is also observed between the peaks of the neat samples and the functionalized form of Pluronic F127. The peaks of the F127-BUM samples are consistently shifted to smaller $q$ values for all three concentrations. This might suggest that the addition of the functional group results in the formation of larger micelles than the neat samples.

In addition to qualitative observations gleaned from the scattering data, important quantitative data can also be obtained to gain further insight into the structure of the hydrogels. The unit cell size ( $a$ ) and the hard sphere diameter ( $D_{HS}$ ) can be determined once the hydrogel structure has been identified. This is accomplished using the first peak's position and Equations 9 and 10 for FCC crystals below[29]:

$$a_{FCC} = \frac{2\pi}{q_{max}}\sqrt{3} \tag{9}$$

$$D_{HS,FCC} = \frac{\pi\sqrt{6}}{q_{max}} \tag{10}$$

**Table 2:** Geometric Parameters for F127 and F127-BUM

| Polymer | Concentration (wt %) | First Peak q ($A^{-1}$) | $a$ (nm) | D Hard Sphere (nm) |
|---|---|---|---|---|
| F127 | 20 | 0.03451 | 31.5 | 22.3 |
| | 25 | 0.04114 | 26.5 | 18.7 |
| | 30 | 0.0441 | 24.7 | 17.5 |
| F127-BUM | 20 | 0.03212 | 33.9 | 23.9 |
| | 25 | 0.03812 | 28.6 | 20.2 |
| | 30 | 0.04081 | 26.7 | 18.9 |

Based on the data in Tables 2, the hard sphere diameter values for neat F127 range from 22.3 nm at 20 wt% to 17.5 nm at 30 wt%. These values are consistent with values seen in literature[37,38]. The range of hard sphere diameter values for F127-BUM gels are slightly larger at 23.9 nm for 20 wt% to 18.9 nm for 30 wt%. This data supports the previous notion that as the polymer concentration is increased for both F127 variants, the micelles are pushed closer together and a reduction in the interstitial cavities are decreased. The ranges between neat F127 and F127-BUM also suggests that the micelles for F127-BUM may be larger due to the absorption of more water.

## 4.2 Polymerization of F127-BUM Hydrogels

Cross-linking is a commonly used method for modifying the properties of polymers within a hydrogel network. By functionalizing Pluronic F127 with bisurethane methacrylate on the end groups, the hydrogel network can be cross-linked by introducing photoinitiator to the solution and exposing the system to UV light (Figure 19).

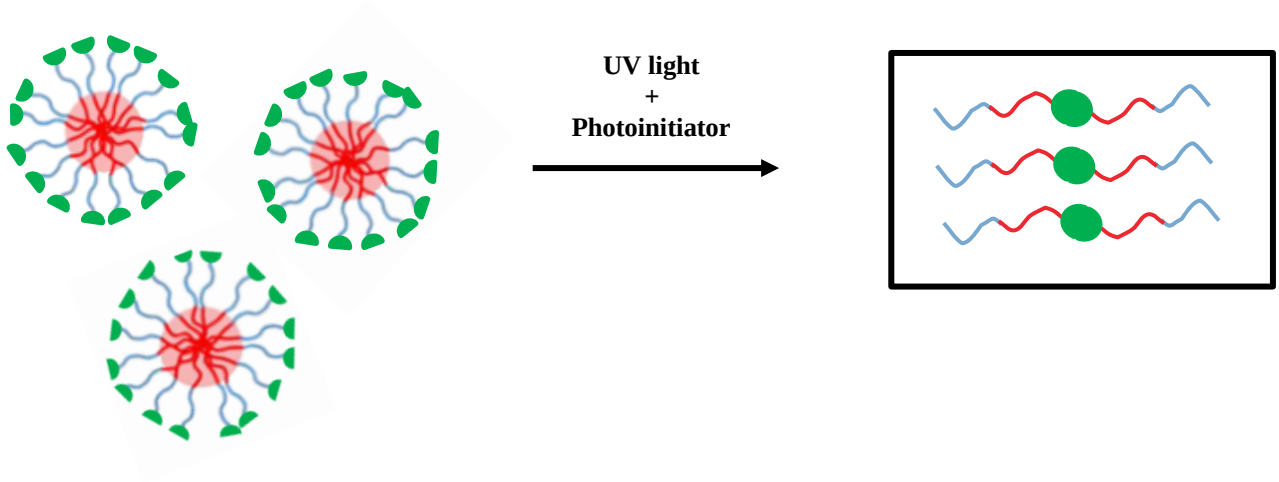


**Figure 19:** Illustration of free radical polymerization of F127-BUM with the introduction of photoinitiator and UV light to the system.
Cross-linking occurs between neighboring bisurethane methacrylate (BUM) end groups.

This process ensures the hydrogel maintains mechanical integrity when exposed to water or media. The process by which F127-BUM hydrogels were cross-linked was through free radical polymerization. Radical polymerization is a common chain-growth polymerization technique that begins with the initiation step, in which free radicals are generated through the decay of a photoinitiator, such as, 2-hydroxy-2-methylpropiophenone. This occurs when the photoinitiator is exposed to UV light. The absorbing molecules are converted to their activated state when photons are absorbed. They rapidly disintegrate into radicals or ions which then initiate polymerization (Figure 20)[39].

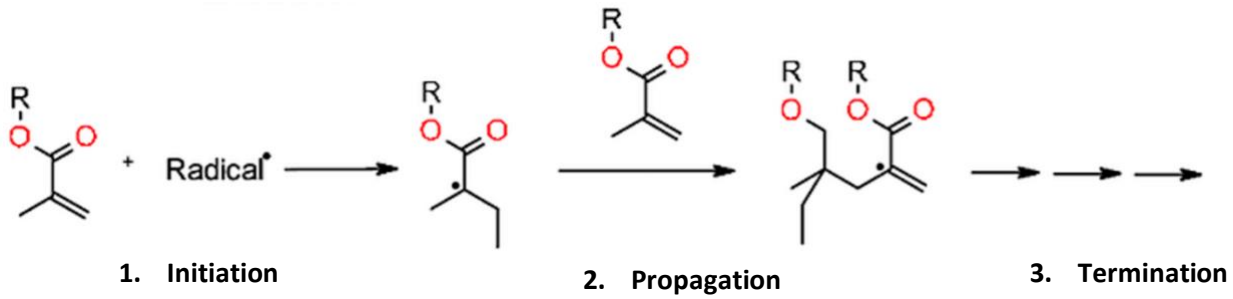


**Figure 20:** General mechanism for radical polymerization.
1) The process begins with the initiation step in which free radicals are generated through the decay of photoinitiator by UV exposure. 2) Next is the propagation step in which the free radicals are added to the double bonds of the monomer to form polymer chains. 3) The process ends with the termination step, where either two radical chains form a single macromolecule or when a hydrogen atom is transferred from one chain to another, leading to one macromolecule.

The process continues with the propagation step, in which the free radicals are added to the double bonds of the monomer to form a polymer chain. The process concludes with the termination step, where either two radical chains form a single macromolecule or when a hydrogen atom is transferred from one chain to another, leading to one macromolecule[39].

Since it was determined functionalizing Pluronic F127 did not result in significant changes to the crystal structure, it was important to determine if the same results would be seen after curing. The circularly averaged scattering profiles for Pluronic F127-BUM gels as well as the cross-linked form for polymer concentrations between 20-30 wt% are shown in Figure 18. The values for each concentration's unit cell size ( $a$ ) and the hard sphere diameter ( $D_{HS}$ ) were also calculated for the cured F127-BUM hydrogels. These values, and how they compare with the values obtained for F127-BUM uncured hydrogels are summarized in Table 3. Based on this data, the hard sphere diameter values for F127-BUM cured gels range from 22.4 nm at 20 wt% to 18.1 nm at 30 wt%. These values are consistently smaller than those of the uncured form.

The trends noted previously when comparing peak positions of F127 neat and F127-BUM are also observed between the F127-BUM uncured and cured gels. The position of the first

peak for all of the F127-BUM cured gels (in blue) show a slight shift to higher *q* for increasing concentrations. This shift suggests that the unit cell of the cubic crystal decreases for increasing polymer concentrations. This is again consistent with interactions between hard spheres. As the concentration of polymer is increased, more polymer micelles are formed and are pushed closer together. Unlike the F127-BUM uncured gels, the cured gels contain photoinitiator and are exposed to UV light. As they are being pushed together, they are forming cross-links between micelles.

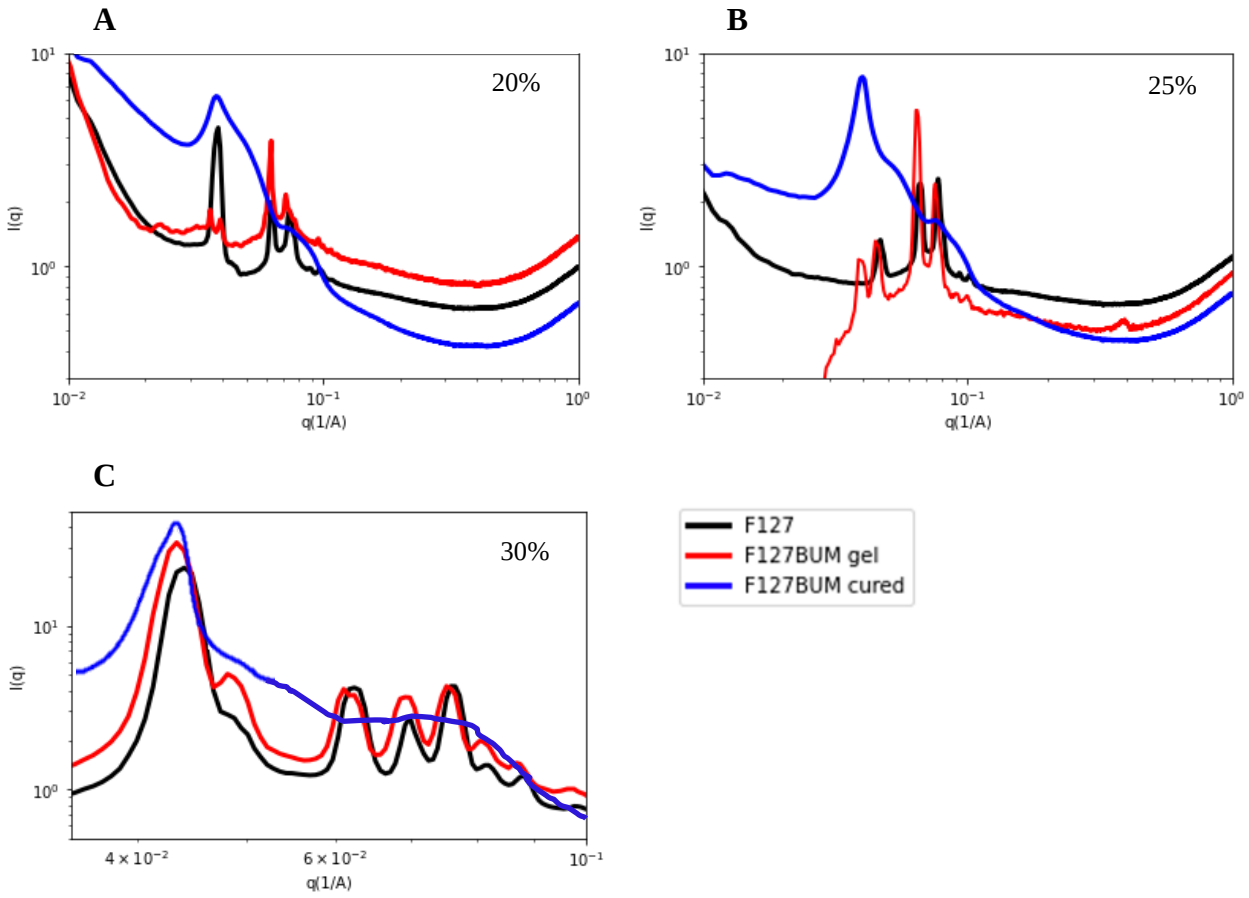


**Figure 21:** X-ray scattering profiles for F127-BUM gels versus cured F127-BUM gels at A) 20 wt%, B) 25 wt%, and C) 30 wt%.

**Table 3:** Geometric Parameters for F127-BUM gels and F127-BUM cured gels.

| Polymer | Concentration (wt %) | First Peak q ($A^{-1}$) | $a$ (nm) | D Hard Sphere (nm) |
|---|---|---|---|---|
| F127-BUM, gel | 20 | 0.03212 | 33.9 | 23.9 |
| | 25 | 0.03812 | 28.6 | 20.2 |
| | 30 | 0.04081 | 26.7 | 18.9 |
| F127-BUM, cured | 20 | 0.03439 | 31.7 | 22.4 |
| | 25 | 0.03901 | 27.9 | 19.7 |
| | 30 | 0.04247 | 25.6 | 18.1 |

Comparing the scattering profile of the F127-BUM gel (in red) to the cured F127-BUM gel (in blue) reveals an obvious loss of the correlation peaks. This suggests that the process of curing the polymer with UV light introduces disorder within the crystal structure, as represented in Figure 22.

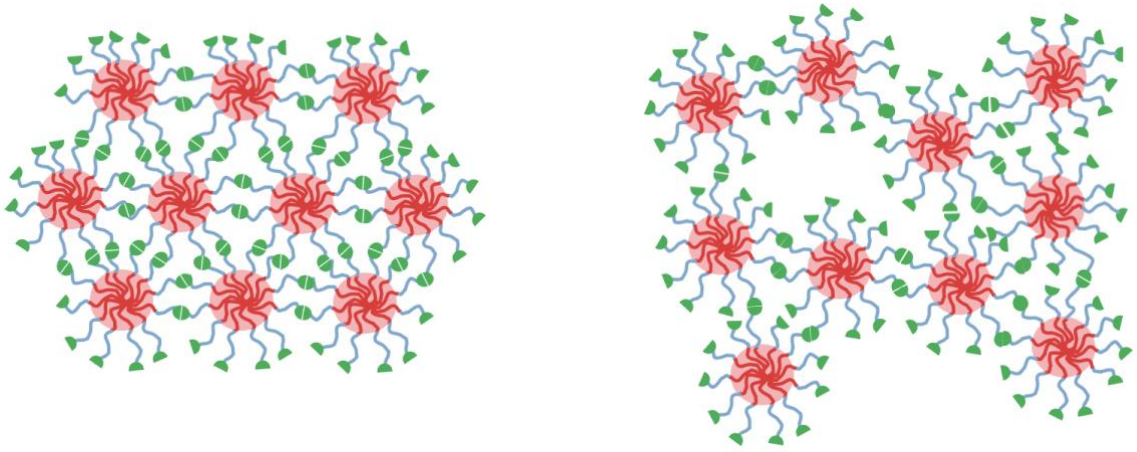


**Figure 22:** Depiction of an ordered and disordered crystal structure within a hydrogel network.

This disorder, which represents a loss of crystallinity within the structure, is consistent with other cross-linked hydrogels. Molecular dynamic simulations performed on cross-linked polyethylene hydrogels suggest that the process of cross-linking decreases crystallinity because cross-links

reduce the amount of crystallizable material available within the system and hinder the mobility of the chains[40]. As more micelles are forming and being pushed closer together, they are also being "frozen" in place as cross-links are formed prematurely, thus forming a non-uniform distribution of cross-links within the hydrogel network.

## 4.3 Lyophilization and Rehydration of F127-BUM Hydrogels

Freeze drying, or lyophilization, is a preferred method in many industries for material preservation and stabilization for extended shelf-life. Additionally, lyophilization has been used to control porosity within hydrogels by varying the water content and the freezing temperature[41].

Cross-linked F127-BUM hydrogels were prepared as previously described. Once the hydrogels were formed, they were placed in a -20°C lab freezer overnight before being placed in the freeze dryer for 24 hours. To determine if the lyophilization process has an effect on the swelling of the F127-BUM hydrogels, swelling studies were performed on both non-lyophilized hydrogels as well as lyophilized (all 30 wt%). The results of this study are presented in Figure 23:

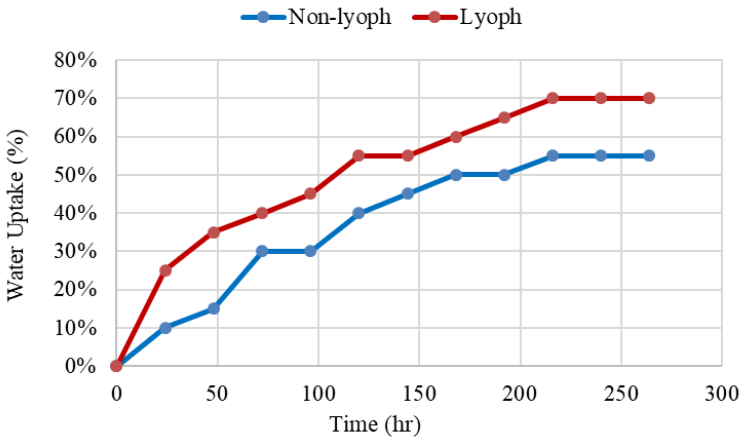


**Figure 23:** Results of swelling studies for lyophilized and non-lyophilized F127-BUM hydrogels. The lyophilized sample consistently absorbed more water at all time stamps when compared to the non-lyophilized sample.

The lyophilized samples not only absorbed a higher percentage of water prior to reaching equilibrium (70% for the lyophilized sample and 55% for the non-lyophilized sample), but they also consistently absorbed higher volumes of water each day. This suggests that the pores within the lyophilized samples may be larger and thus able to absorb more water than the non-lyophilized counterpart.

To further investigate the effect that lyophilization and rehydration have on F127-BUM hydrogels, small angle X-ray scattering was used to probe cured hydrogels before (Sample 1) and after lyophilization (Sample 2), after the hydrogels were submerged in water and equilibrium was reached (Sample 3), and again several weeks past the equilibrium state (Sample 4). Photographs of each sample is shown in Figure 24. All samples were 30 wt%. The scattering results are shown in Figure 25.

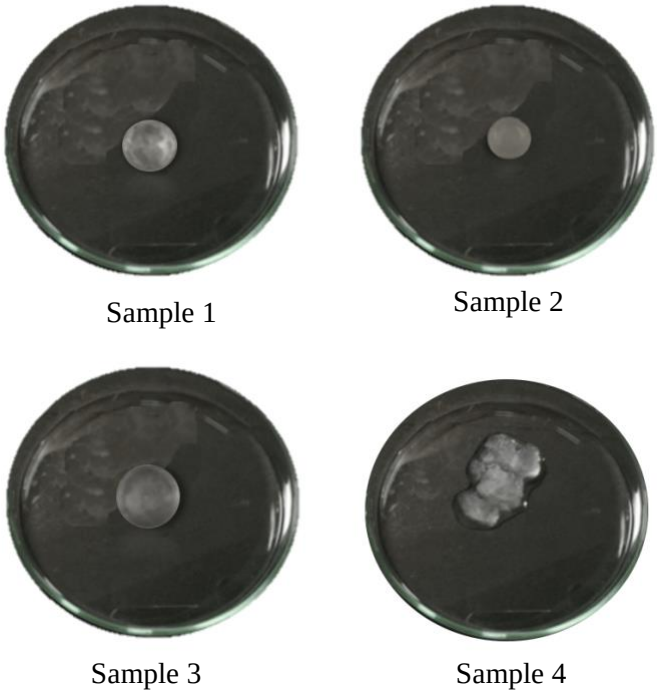


**Figure 24:** Representative photographs of hydrogels for each experimental condition. Sample 1 is a cured 30 wt% sample prior to lyophilization. Sample 2 is the same hydrogel after lyophilization. Sample 3 is a non-lyophilized hydrogel after equilibrium is reached in water. Sample 4 is the lyophilized sample several weeks after reaching equilibrium. All structural integrity is lost in this sample.

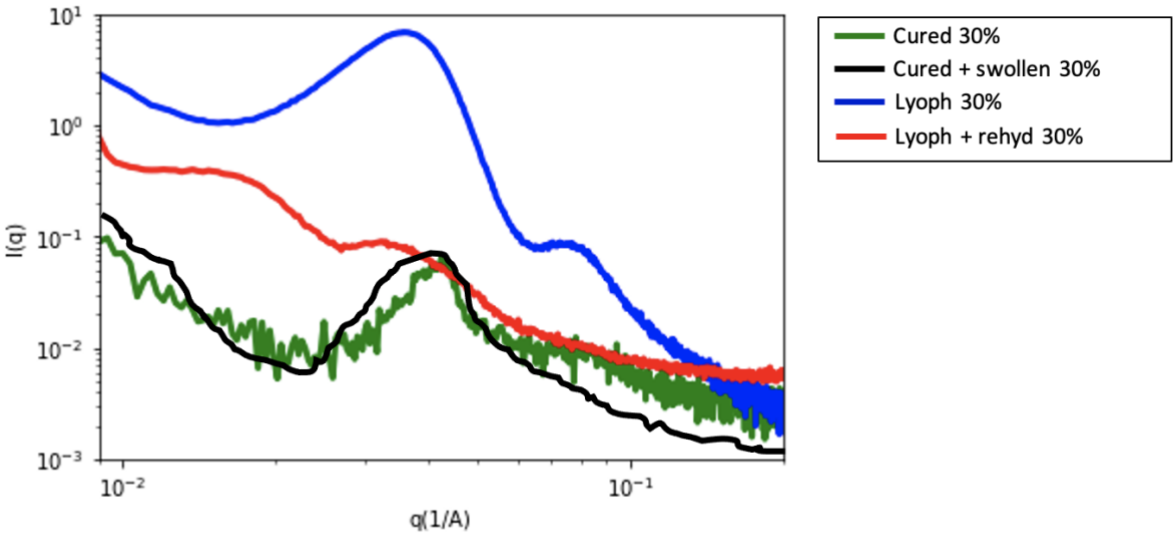


**Figure 25:** Small angle X-ray scattering data for lyophilization and rehydration study. Green line represents the initial cured 30 wt% hydrogel, prior to lyophilization. Blue line represents the same hydrogel after lyophilization. Black line represents a non-lyophilized sample that has been swollen with water and reached equilibrium. Red line represents the lyophilized sample several weeks after reaching equilibrium with water.

The scattering data for all samples, with the exception of the lyophilized and rehydrated sample (in red), have similar profiles to those seen in the previous section. They all have the same slightly reduced correlation peaks consistent with the loss of order that is introduced by the polymerization process. However, the correlation peaks for the lyophilized and hydrated sample (in red) shows a significant flattening of the peaks, suggesting that even more disorder is introduced post-swelling.

The photograph for the lyophilized sample after reaching a state of equilibrium with water shows a slightly larger volume than the original cured sample prior to lyophilization. This is consistent with the results obtained from the swelling study. What is most interesting to note is the lyophilized sample many weeks after reaching equilibrium. This sample has lost all structural integrity. Since polymerization was found to introduce disorder within the crystal structure of the F127-BUM hydrogels, it seems that the way in which samples were prepared for lyophilization could be a contributing factor to an observed increase in disorder.

Research suggests that the initial temperature that is used to freeze hydrogels has a significant effect on the pore size within the hydrogel[41]. The pore size can ultimately influence the amount of water that can be retained in the hydrogel. A study conducted by H. Kang, et al. showed that when gels were frozen below 0°C, water inside the gel transformed into ice crystals. The lyophilization process turns these ice crystals directly into vapor through sublimation and the spaces previously occupied by ice becomes pores. When the hydrogels were frozen at -20°C, the water within the gel froze slowly into ice crystals. As a result, the crystals were able to grow in size resulting in larger pores left in the hydrogel. When the hydrogels were frozen at much lower temperatures like -196°C (the temperature of liquid nitrogen), the water transformed into ice crystals instantaneously. This left no time for the ice crystals to grow in size and thus resulted in smaller pores left in the gel. The researchers concluded that by adjusting the initial freezing temperature experienced, one could tune the size of the pores within the hydrogels. The lower the freezing temperature, the smaller the pore sizes. Since samples were initially frozen at -20°C, the water contained within the hydrogel froze slowly into ice crystals[41]. The ice crystals were able to grow in size and produce larger pores. This may have compounded the original disorder within the crystal lattice, allowing even more water to enter the hydrogel network.

# Chapter 5: Future Work

## 5.1 Improvements to Lyophilization Process

The research presented in this thesis investigated the effects of functionalization, polymerization, and lyophilization and rehydration on Pluronic F127-BUM hydrogels. It was determined that lyophilized samples experienced loss of structural integrity when re-exposed to water many weeks beyond the point when equilibrium was reached. Samples that were not lyophilized but were exposed to water for the same amount of time as the lyophilized samples did not experience the same degradation. This suggests that the lyophilization process may be compounding the effects of the disorder that is initially introduced from the polymerization process. Based on these results, hydrogels may benefit from lower initial freezing temperatures. Future experimentation should include freezing hydrogels at much lower temperatures, perhaps with liquid nitrogen, to determine if the mechanical properties of the hydrogels are preserved.

## 5.2 Prevention of Cell Leakage

It was determined that the process of polymerizing to form permanent hydrogels introduces defects within the crystal lattice. Originally, it was hypothesized that these defects could be the source of a continued problem of cell leakage that has consistently been observed throughout the collaborative investigation of the microbe-laden hydrogels (Figure 26). Figure 26-A represents the initial time point when the microbe-laden hydrogel is placed in solution. Figure 26-B represents the final state after cell leakage occurs.

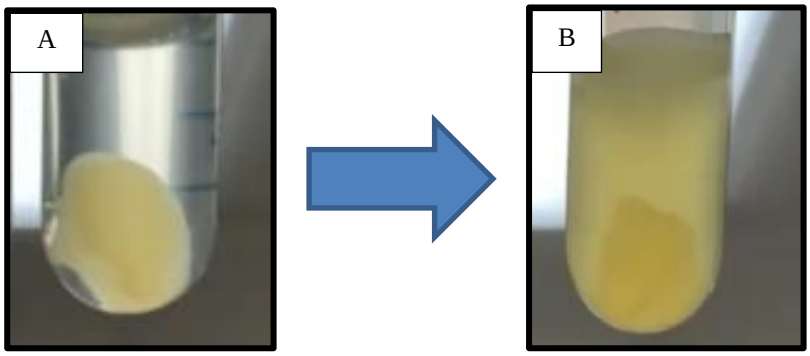


**Figure 26:** Photographic depiction of cell leakage from F127-BUM cross-linked hydrogels. Photos provided by the Alper Group.

Ultra-small angle X-ray scattering (USAXS) was used to probe the hydrogels at very small *q*-values. Since *q*-values have units of inverse length, a small *q*-range corresponds to larger length scales. These larger length scales are necessary to observe the hydrogels at length scales equivalent to the microbes that would be encapsulated within hydrogel network. Figure 27 shows the USAXS results obtained for 30 wt% F127-BUM gel and F127-BUM cross-linked hydrogel. Although the scattering profile does reveal a defect at a smaller *q*-range (between 0.003 and 0.01 $Å^{-1}$), this is not the equivalent length scale of the microbes. The length scales and corresponding *q*-values for the microbes are summarized in Table 4.

**Table 4:** Length scales of *S. cerevisiae* and *E. coli*

| **Microbe** | **Approximate size (nm)** | ***q*-value ($Å^{-1}$)** |
|---|---|---|
| Bacteria, *E. coli* | 1,000 | $6 \times 10^{-4}$ |
| Yeast, *S. cerevisiae* | 5,000 | $2 \times 10^{-4}$ |

The *q*-values for both microbes are much smaller than what is represented by the x-axis in Figure 27. This means that the length scale range for the defect (~ 628 - 2094 nm) is much smaller than

the microbes. Therefore, it cannot be concluded that the disorder due to polymerization is the cause of the cell leakage.

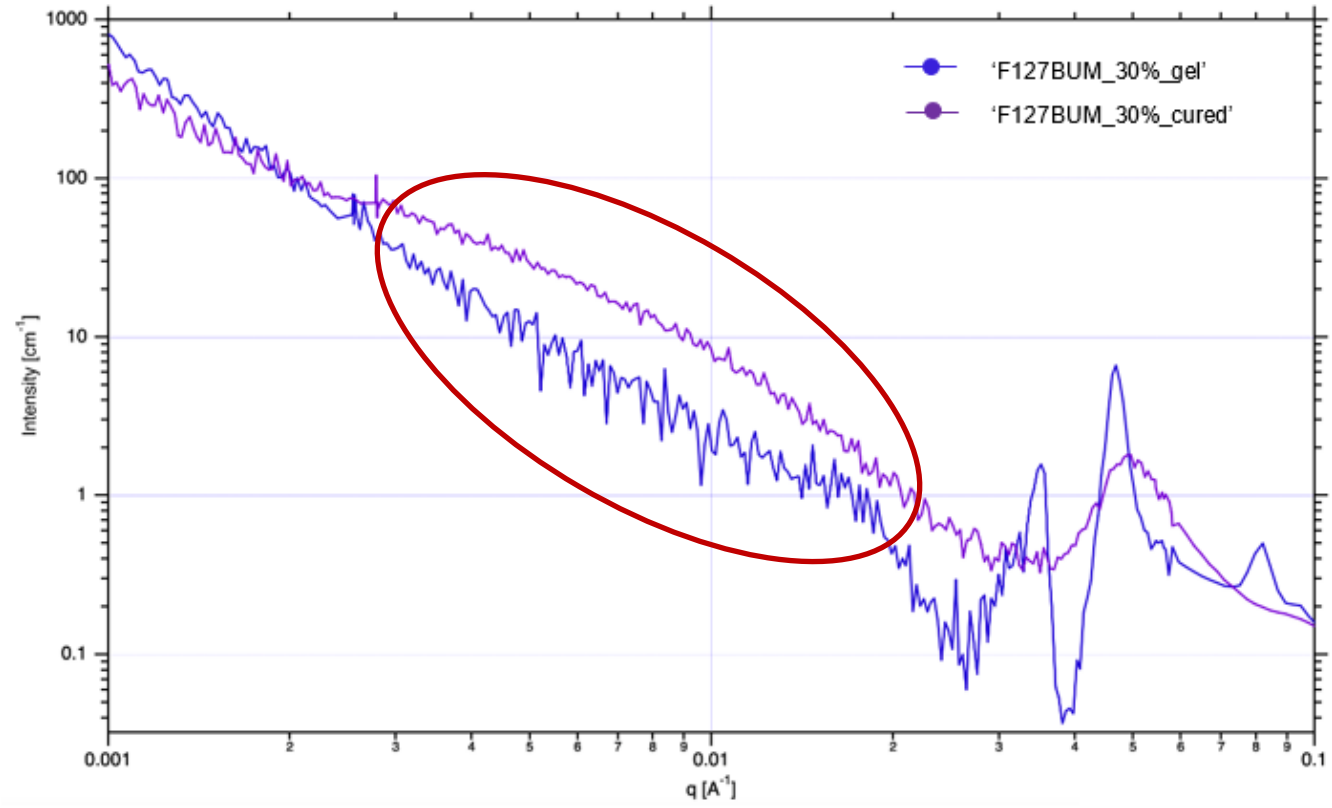


**Figure 27:** Ultra small angle X-ray scattering profile of 30 wt% F127-BUM gel and F127-BUM cured hydrogel.
Red circle highlights a defect that is consistently observed in cured F127-BUM hydrogels.

Early attempts were made to prevent or slow down the rate of cell leakage of the F127-BUM hydrogels by dip coating them with cross-linked sodium alginate gels. To determine if this was a viable solution, sodium alginate hydrogels cross-linked with calcium chloride at various weight concentrations (2, 3, and 4 wt%) were subjected to small angle X-ray scattering experiments. The scattering profiles obtained from this experiment are summarized in Figure 28:

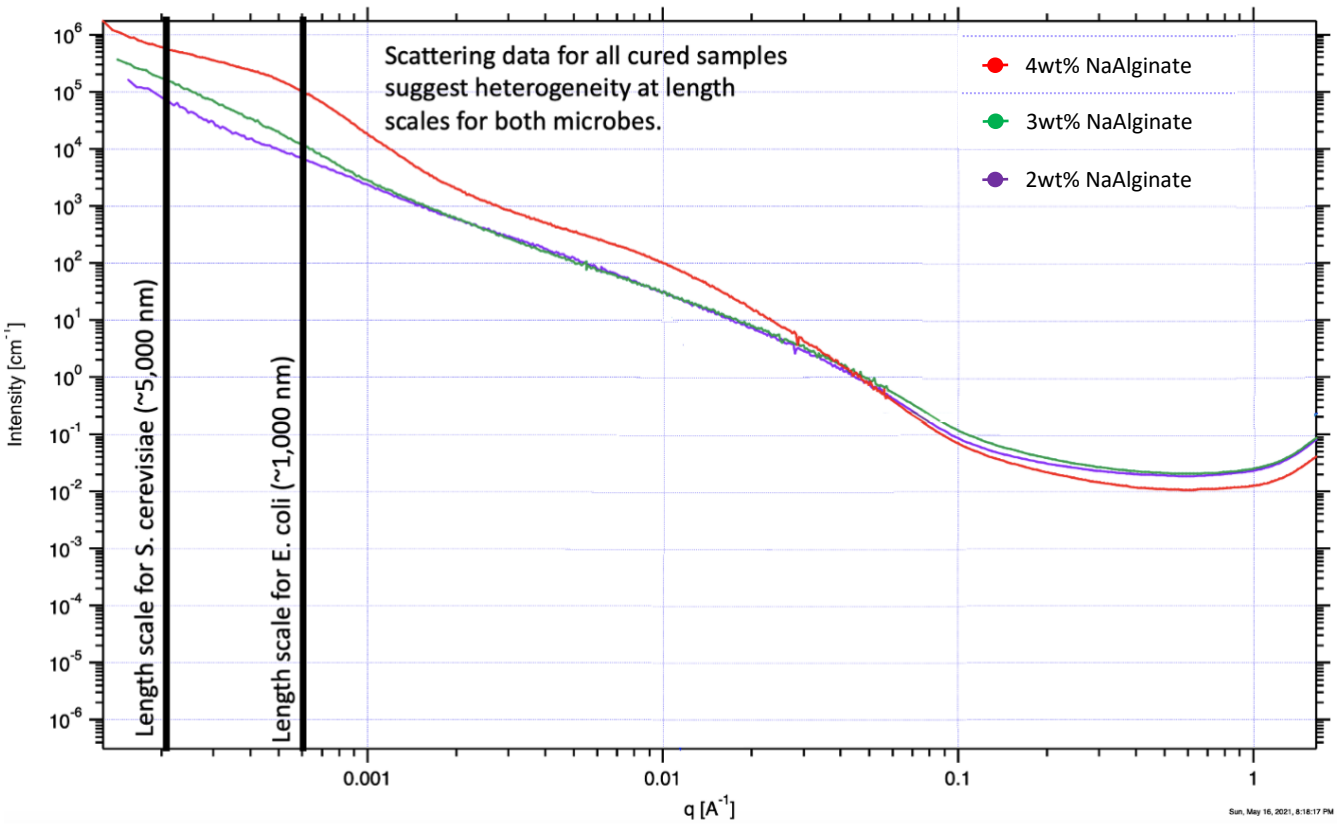


**Figure 28:** USAXS scattering profiles of sodium alginate gels of 2, 3, and 4 wt%. The data shows heterogeneities for all gels at *q*-values with length scales equivalent to those of the microbes.

Unfortunately, these results show that heterogeneities of the cured samples exist at the same length scale of the microbes. Therefore, sodium alginate coatings are not capable of preventing cell leakage. Although sodium alginate was not a viable solution, future experiments should be designed to include additional hydrogel coatings. It is imperative that the source of the cell leakage is determined and controlled.

## 5.3 Correlate Hydrogel Defects with Diffusion Rates

High throughput experimentation (HTE) was used in preliminary experiments to determine the diffusion rates of cross-linked F127-BUM hydrogels at different weight concentrations using

Beer's law and UV-Vis. A simplified outline of the experimental procedure is shown in Figure 29 and the results of the experiment are summarized in Figure 30.

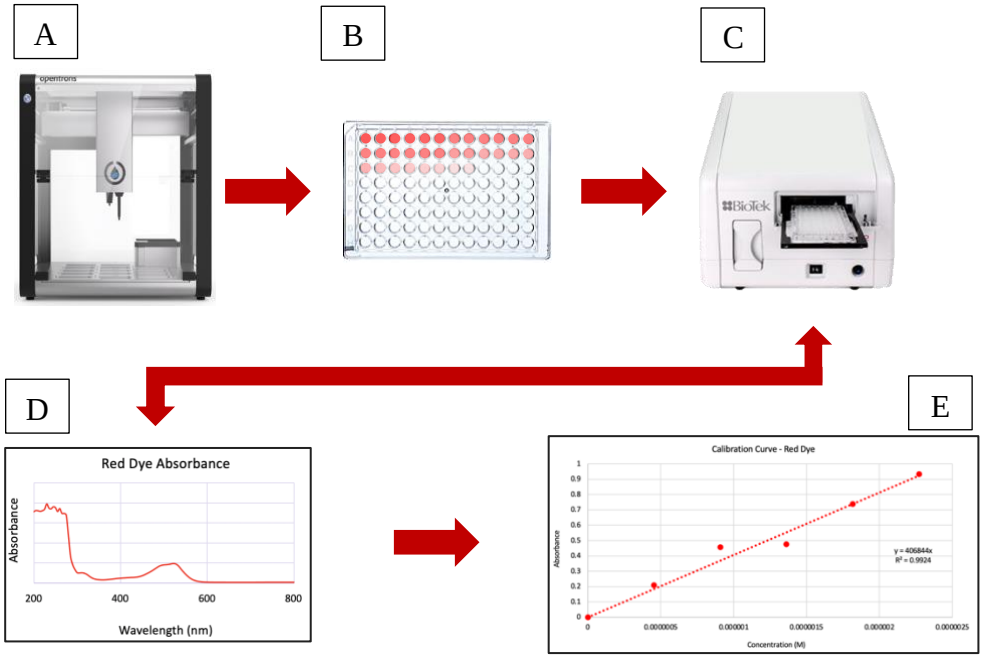


**Figure 29:** High throughput experimentation to determine diffusion rates of hydrogels at various weight concentrations.
A) Liquid handling robot was used to both make hydrogel samples at various weight concentrations as well as dispense red dye onto the hydrogels at defined time intervals, B) Hydrogels exposed to red dye at 600 second intervals, C) Absorbance readings were obtained via UV-Vis, D) Peak absorbance for each sample was used to determine the concentration of red dye that had diffused into the hydrogel, and E) Beer's law and samples of known concentrations were used to generate a calibration curve to calculate the concentration of red dye in each hydrogel sample.

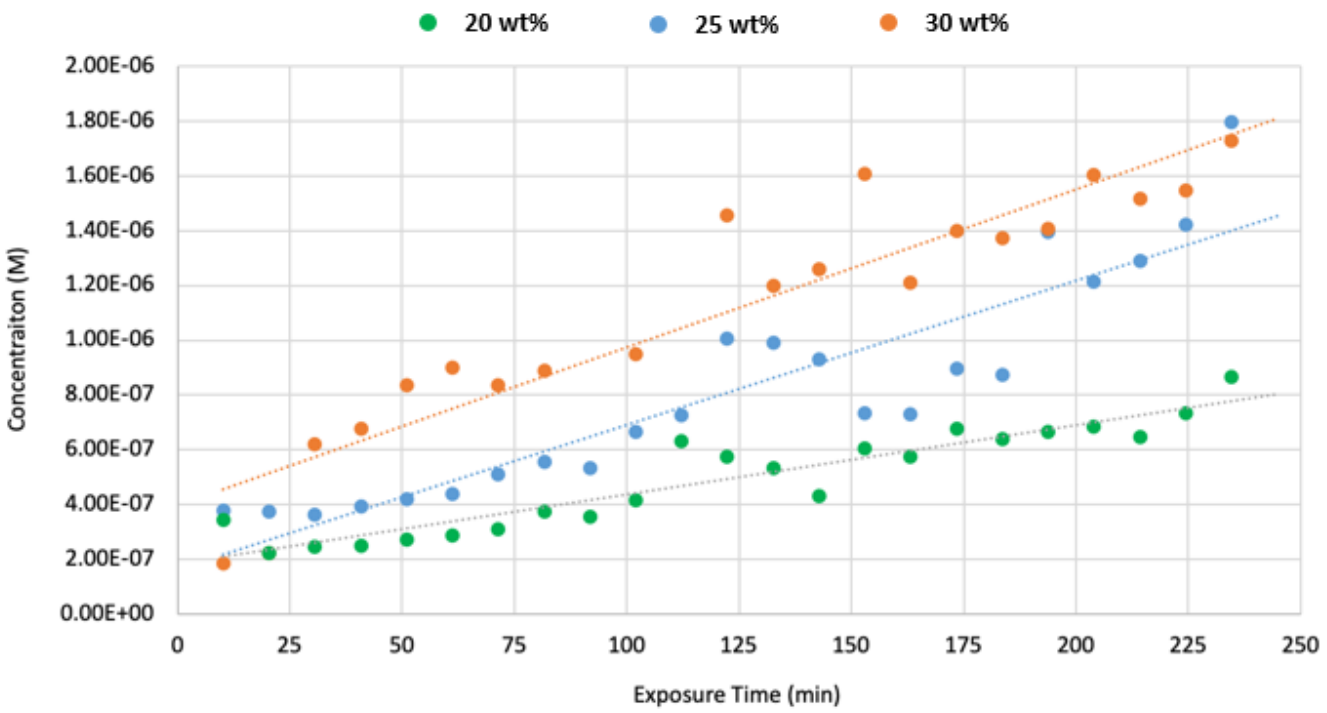


**Figure 30:** Results obtained from diffusion experiments.
30 wt% hydrogels (in orange) consistently had higher rates of diffusion when compared to results for 20 wt% (in green) and 25 wt% (in blue).

Similar experiments should be performed in the future to determine if the defects that are introduced into the crystal structure of F127-BUM hydrogels from the polymerization process have any significant effect on the diffusive performance of the hydrogels. This method could also be repeated with microbe-laden hydrogels to measure the extent of cell leakage over time.

## Chapter 6: Conclusions

The work presented in this thesis focused on using small angle X-ray scattering to characterize the progression of F127 through functionalization with bisurethane methacrylate to form F127-BUM, polymerization into cured hydrogels to prevent dissolution in water, and lyophilization/rehydration for extended shelf life. The initial study of F127-BUM supported the gelation and rheological results obtained by the Nelson group. The process of functionalizing F127 had very little effect on its crystal structure or gelation properties. These results were supported by scattering profiles obtained from SAXS. Both F127 neat and F127-BUM gels showed scattering profiles consistent with a face-centered cubic crystal lattice. The second study revealed that the process of polymerizing F127-BUM with UV light did alter the crystal structure significantly by introducing disorder into the crystal lattice. The correlation peaks for cured samples were consistently lost for all weight concentrations. The final study revealed that the process of lyophilizing and rehydrating the F127-BUM hydrogels compounded the previous findings. The disorder was intensified and led to a complete loss of structural integrity.

## Chapter 7: References


[1] Jung, Young-seok, et al. (2017). Thermo-sensitive injectable hydrogel based on the physical mixing of hyaluronic acid and Pluronic F-127 for sustained NSAID delivery. *Carbohydrate Polymers, 156,* 403-408. https://doi.org/10.1016/j.carbpol.2016.08.068

[2] Bahram, Morteza, et al. (2016). An Introduction to Hydrogels and Some Recent Applications. *Emerging Concepts in Analysis and Applications of Hydrogels.* DOI: 10.5772/64301

[3] Parhi, Rabinarayan, et al. (2017) Cross-Linked Hydrogel for Pharmaceutical Applications: A Review. *Advanced Pharmaceutical Bulletin*, *7*(4), 515-530. DOI:10.15171/apb.2017.064

[4] M. Yokoyama, et al. (1990). Characterization and anticancer activity of the micelle-forming polymeric anticancer drug adriamycin-conjugated poly(ethylene glycol)-poly(aspartic acid) block copolymer. *Cancer Research*, *50*(6), 1693-1700.

[5] S. Skaalure, et al. (2104). An Enzyme-Sensitive PEG Hydrogel Based on Aggrecan Catabolism for Cartilage Tissue Engineering. *Advanced Healthcare Materials, 4*(3), 420-431. DOI: 10.1002/adhm.201400277

[6] Xinyue Liu, et al (2022). Engineered Living Hydrogels. *Advanced Materials, 36*(6). https://doi.org/10.1002/adma.202201326

[7] A. Courbet, et al. (2015). Detection of pathological biomarkers in human clinical samples via amplifying genetic switches and logic gates. *Science Translational Medicine, 7*(289), 283-289. DOI: 10.1126/scitranslmed.aaa3601

[8] Brooks, S, et al. (2022). Enhancing long-term storage and stability of engineered living materials through desiccant storage and trehalose treatment. *Biotechnology and Bioengineering*, 1-11. https://doi.org/10.1002/bit.28271

[9] Ro, D.K., et al. (2006). Production of the Antimalarial Drug Precursor Artemisinic Acid in Engineered Yeast. *Nature, 440*(7086), 940-943. https://doi.org/10.1038/nature04640.

[10] Christen, C. (2021, March 17). *Meat Consumption in the U.S. Is Growing at an Alarming Rate*. Sentient Media. https://sentientmedia.org/meat-consumption-in-the-us/

[11] Conzachi, K. (2022, March 15). *It May Be Uncomfortable, But We Need to Talk About It: The Animal Agriculture Industry and Zero Waste*. University of Colorado Boulder. https://www.colorado.edu/ecenter/2022/03/15/it-may-be-uncomfortable-we-need-talk-about-it-animal-agriculture-industry-and-zero-waste#:~:text=Raising%20livestock%20for%20human%20consumption,biodiversity%20loss%2C%20and%20water%20pollution.

[12] Butelmann, T., et al. (2021). Metabolism Control in 3D-Printed Living Materials Improves Fermentation. *ACS Applied Biomaterials*, 4, 7195-7203. https://doi.org/10.1021/acsabm.1c00754?urlappend=%3Fref%3DPDF&jav=VoR&rel=cite-as

[13] Pitto-Barry, A., et al. (2014). Pluronic® block-copolymers in medicine: from chemical and biological versatility to rationalisation and clinical advances. *Polymer Chemistry*, *10*, 3291-3297. https://doi.org/10.1039/C4PY00039K

[14] Sharma, R., et al. (2014). Polyethylene Oxide-Polypropylene Oxide Based Block Copolymers as Nanovehicles for Drug Formulations. *BioEvolution, 1*(3), 68-75.

[15] Alexandridis, P., et al. (1994). Micellization of Polyethylene oxide)-Poly(propylene oxide)-Poly(ethylene oxide) Triblock Copolymers in Aqueous Solutions: Thermodynamics of Copolymer Association. *Macromolecules, 27*(9), 2414-2425. https://doi.org/10.1021/ma00087a009

[16] Meznarich, N. Effect of ternary solutes on the evolution of structure and gel formation in amphiphilic copolymer solutions: University of Michigan; 2012.

[17] Vadnere, M., et al. (1984). Thermodynamic studies on the gel-sol transition of some Pluronic polyols. *International Journal of Pharmaceutics*, *22*(2-3), 207-218. https://doi.org/10.1016/0378-5173(84)90022-X

[18] McConnell, G., et al. (1993). Disorder-order transitions in soft sphere polymer micelles. *Physical Review, 71*(13), 2102-2105. DOI: 10.1103/PhysRevLett.71.2102

[19] Hamley, I. W., et al. (1998). Effect of shear on cubic phases in gels of a di-block copolymer. *The Journal of Chemical Physics*, *108*(16), 6929-6936. https://doi.org/10.1063/1.476108

[20] Mortensen, K., et al. (1996). Structural studies of aqueous solutions of PEO-PPO-PEO triblock copolymers, their micellar aggregates and mesophases; a small-angle neutron scattering study. *Journal of Physics: Condensed Matter, 8*, A103-A124. DOI:10.1088/0953-8984/8/25A/008

[21] Prudhomme, R. K., et al. (1996) Structure and Rheology Studies of Poly(oxyethylene−oxypropylene−oxyethylene) Aqueous Solution. *Langmuir, 12*(20), 4651-4659. https://doi.org/10.1021/la951506b

[22] Wu, C., et al. (1997) Characterization of the PEO−PPO−PEO Triblock Copolymer and Its Application as a Separation Medium in Capillary Electrophoresis. *Macromolecules, 30*(16), 4574-4583. https://doi.org/10.1021/ma9701088

[23] Mortensen, K., et al. (2008) Effects of PEO-PPO Diblock Impurities on the Cubic Structure of Aqueous PEO-PPO-PEO Pluronics Micelles: fcc and bcc Ordered Structures in F127. *Macromolecules, 41*(5), 1710-1727. https://doi.org/10.1021/ma702269c

[24] Diniz, I., et al. (2015) Pluronic F-127 hydrogel as a promising scaffold for encapsulation of dental-derived mesenchymal stem cells. *J. Mater. Sci, 16*(53), https://doi.org/10.1007/s10856-015-5493-4

[25] Cidade, M.T., et al. (2019) Injectable Hydrogels Based on Pluronic/Water Systems Filled with Alginate Microparticles for Biomedical Applications. *Materials, 12*(7). https://doi.org/10.3390/ma12071083

[26] Priks, Hans, et al. (2020) Physical confinement impacts cellular phenotypes within living materials. *ACS Applied Biomaterials, 3*(7), 4273–4281. https://doi.org/10.1021/acsabm.0c00335

[27] SAXS nanostructure analysis. (n.d.). *Anton Paar*. https://wiki.anton-paar.com/us-en/saxs-nanostructure-analysis/

[28] Hammouda, B. Probing Nanoscale Structures - The SANS Toolbox. https://www.ncnr.nist.gov/staff/hammouda/the_SANS_toolbox.pdf

[29] Pozzo, D. (2006). *Templating Nanoparticles using Thermo-Reversible Soft Crystals* (Publication # 3211190) [Doctoral dissertation, Carnegie Mellon University]. ProQuest Information and Learning Company.

[30] Pauw, B. (2013) Everything SAXS: small-angle scattering pattern collection and correction. *Journal of Physics: Condensed Matter, 25*. doi:10.1088/0953-8984/25/38/383201

[31] Monodisperse spheres. (February 2008). *NIST SANS Model Function Documentation*. https://www.ncnr.nist.gov/programs/sans/data/Download/SANS_Model_Docs_v4.00.pdf

[32] CoreShell. (February 2008). *NIST SANS Model Function Documentation*. https://www.ncnr.nist.gov/programs/sans/data/Download/SANS_Model_Docs_v4.00.pdf

[33] Costanzo, S., et al. (2021) Rheology and morphology of Pluronic F68 in water. *Physics of Fluids, 33*, 043113-1 – 043113-10. https://doi.org/10.1063/5.0049722

[34] Pozzo, L. SAXS-USAXS Liquids 48 well plate holder. https://github.com/pozzo-research-group/Automation-Hardware/

[35] Karis, D. (2020). *Crosslinking Methods for 3D Printable Hydrogel Materials.* [Doctoral dissertation, University of Washington]. ProQuest Information and Learning Company.

[36] Callister, W. D. (2009). *Materials science and engineering: An introduction* (8th ed.). John Wiley & Sons, Inc.

[37] Basak, R., et al. (2013). Encapsulation of Hydrophobic Drugs in Pluronic F127 Micelles: Effects of Drug Hydrophobicity, Solution Temperature, and pH. *Langmuir, 29*(13), 4350-4356. https://doi.org/10.1021/la304836e

[38] Vaidya, F., et al. (2018). Pluronic micelles encapsulated curcumin manifests apoptotic cell death and inhibits pro inflammatory cytokines in human breast adenocarcinoma cells. *Cancer Reports, 2*(1). https://doi.org/10.1002/cnr2.1133

[39] Lee, J., et al. (2001). Cure depth in photopolymerization: Experiments and theory. *Materials Research Society, 16*(12), 3536-3544. https://doi.org/10.1557/JMR.2001.0485

[40] Paajanen, A., et al. (2019). Crystallization of cross-linked polyethylene by molecular dynamics simulation. *Polymer, 171*, 80-86. https://doi.org/10.1016/j.polymer.2019.03.040

[41] Kang, H., et al. (1999). Effect of Porous Structure on the Degradation of Freeze-Dried Gelatin Hydrogels. *Journal of Bioactive and Compatible Polymers, 14*(4), 291-367. https://doi.org/10.1177/088391159901400404